INRIA

UNITÉ DE RECHERCHE
INRIA-SOPHIA ANTIPOLIS

Institut National
de Recherche
en Informatique
et en Automatique

Domaine de Voluceau
Rocquencourt
BP 105
78153 Le Chesnay Cedex
France
Tél. (1) 39 63 55 11

Rapports de Recherche

N° 1175

Programme 7
Calcul Scientifique,
Logiciels Numériques et Ingénierie Assistée

ON TVD CRITERIA FOR MESH ADAPTION FOR EULER AND NAVIER-STOKES CALCULATIONS

Bernadette PALMERIO
Loula FEZOUI
Christian OLIVIER
Alain DERVIEUX

Mars 1990

RR-1175

ON TVD CRITERIA FOR MESH ADAPTION FOR EULER AND NAVIER-STOKES CALCULATIONS

CRITERES TVD D'ADAPTATION DE MAILLAGE POUR LA RESOLUTION DES EQUATIONS D'EULER ET DE NAVIER-STOKES

Bernadette PALMERIO (*)
Loula FEZOUI (**)
Christian OLIVIER (**)
Alain DERVIEUX (**)
(*) Université de Nice et INRIA-Sophia-Antipolis
(**) INRIA-Sophia-Antipolis, B.P.109, 06560 VALBONNE, FRANCE

ABSTRACT

Considering the TVD methods as accuracy-adaption methods, we propose a strategy for deciding mesh refinements for TVD-approximated compressible flows. Both mesh enrichment and deformation are applied to typical test cases involving shocks boundary layers : a flow past a flat plate and flows around an airfoil.

RESUME

On propose une stratégie de raffinement de maillage basée sur la précision TVD, pour résoudre des écoulements compressibles calculés par un schéma TVD. Enrichissement et Déplacement de maillage sont tous deux appliqués à des cas tests comportant chocs, couches limites : Ecoulement le long d'une plaque plane et des écoulements autout d'un profil NACA0012.

INTRODUCTION

From many years, the occuring of oscillations in numerical solutions of viscous layers have been an important problem in CFD. The CFD community where advised by Ph. Gresho and R. Lee [1] not to "suppress the wiggles" because they were "telling us something". In this paper, we suggest to listen what they are telling and then to anyway suppress them.

They are telling "the mesh is not fine enough here". Then we can :

- either adapt the approximation by degrading it to a first-order accurate diffusive one (this point of view is exactly the opposite of the p-method!),
- or adapt the mesh (applying a h-method).

We propose to apply both strategies : indeed, if the mesh is not adapted, the accuracy is not good ; if the first-order diffusive approximation is not applied, the preliminary solution oscillates, and this may result in divergence of the solution algorithm, particularly in hyperbolic compressible models.

In the TVD-mesh-adaption method that we propose, when the possible arising of oscillation is detected by applying the TVD principle, an ad hoc diffusion is added and mesh refinement is decided. An ideal situation would be obtained when all TVD-limited regions of the computational domain are refined until the approximation is second-order accurate everywhere. This is the ultimate goal of the work presented.

1. THE TVD SCHEME

We first shortly define the scheme that is used for the calculation of the flow ; this kind of scheme has been introduced in [5] ; a more complete description can be found in [4].

The 2-D Navier-Stokes equations is written in short as follows :

$$\frac{\partial W}{\partial t} + \frac{\partial F(W)}{\partial x} + \frac{\partial G(W)}{\partial y} = \frac{1}{Re}\left(\frac{\partial R(W)}{\partial x} + \frac{\partial S(W)}{\partial y}\right), \tag{1}$$

in which $W(x,y,t)$ is a vector function in R^4 :

$$W = \begin{pmatrix} \rho \\ \rho u \\ \rho v \\ E \end{pmatrix} \tag{2}$$

where ρ is the density, u and v are the components of the velocity and E the total energy per volume unit. $F(W)$ and $G(W)$ are given by :

$$F(W) = \begin{pmatrix} \rho u \\ \rho u^2 + p \\ \rho uv \\ (E+p)u \end{pmatrix} \quad G(W) = \begin{pmatrix} \rho v \\ \rho uv \\ \rho v^2 + p \\ (E+p)v, \end{pmatrix} \tag{3}$$

where p is the pressure defined by the perfect gas law ($\gamma = 1.4$) :

$$p = (\gamma - 1)\left(E - \frac{1}{2}\rho(u^2 + v^2)\right). \tag{4}$$

$R(W)$ and $S(W)$ are the diffusive flux functions, defined as follows :

$$R(W) = \begin{pmatrix} 0 \\ \tau_{xx} \\ \tau_{xy} \\ u\tau_{xx} + v\tau_{xy} + \dfrac{\gamma k}{Pr}\dfrac{\partial \varepsilon}{\partial x} \end{pmatrix} \quad S(W) = \begin{pmatrix} 0 \\ \tau_{xy} \\ \tau_{yy} \\ u\tau_{xy} + v\tau_{yy} + \dfrac{\gamma k}{Pr}\dfrac{\partial \varepsilon}{\partial y}. \end{pmatrix} \tag{5}$$

ε is the specific internal energy ; T is the temperature, k is a normalised thermal conductivity, τ_{xx}, τ_{xy} and τ_{yy} are the components of the stress tensor.

For Euler calculations we put $R(W) = S(W) = 0$.

Numerical integration

The integration domain is assumed to be a polygon, divided in a classical finite-element triangulation. The degrees of freedom are the values of W on each vertex. The dual finite-volume mesh is defined from cells C_i around each vertex i drawn with sections of the surrounding medians (Figure 1). These volumes will be used for the integration of the time derivative and of the advection terms.

The viscous terms are discretised by applying the usual Galerkin variational method. Then we can write the approximation as follows :

$$\begin{aligned} &aire\,(C_i)\,\frac{W_i^{n+1} - W_i^n}{\Delta t^n} + \int_{\partial C_i} \mathcal{F}\,(W, \vec{\eta})\,d\sigma = \\ &-\frac{1}{Re}\sum_{T, i \in T} \iint_T \left(R\frac{\partial \varphi_i}{\partial x} + S\frac{\partial \varphi_i}{\partial y} \right) dxdy + boundary\ integral\ , \end{aligned} \tag{6}$$

in which φ_i hold for the P_1 Galerkin basis functions, the sum is taken over the triangles having i as a vertex, and

$$\mathcal{F}\,(W, \vec{\eta}) \;=\; F\,\eta_x \;+\; G\,\eta_y \tag{7}$$

The advection terms are discretised by a finite-volume scheme that is compatible with the Galerkin finite-element for advection [9]. The flux are computed through the boundary of cells defined by centroids and mid-sides (Figure 1)

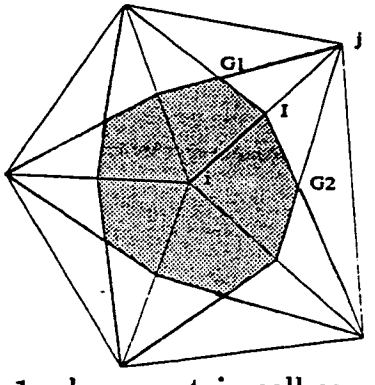

Figure 1 : barycentric cell around a vertex

$$\int_{\partial C_i} \mathcal{F}(W,\vec{\eta})\, d\sigma = \sum_{j \epsilon K(i)} \int_{\partial C_{ij}} \mathcal{F}(W,\vec{\nu})\, d\sigma + \int_{\partial C_i \cap \Gamma_h} \mathcal{F}(W,\vec{\eta})\, d\sigma \ , \qquad (8)$$

where $K(i)$ holds for the set of vertices that are neighbors of vertex i, $\Gamma_h = \partial\Omega_h$, et $\partial C_{ij} = \partial C_i \cap \partial C_j = [G_{1,ij}, I_{ij}] \cup [I_{ij}, G_{2,ij}]$ (see Figure 2).

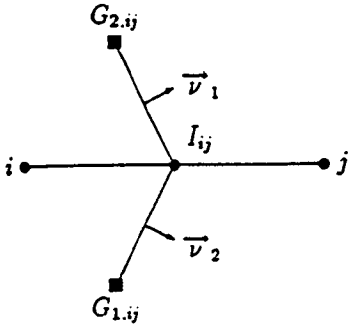

Figure 2 : Flux integration between two cells

where the sum is taken over the neighbouring vertices j around vertex i. Then each flux between cell i and cell j is computed through an approximate Riemann solver which define a flux function :

$$\int_{\partial C_{ij}} \mathcal{F}(W,\vec{\nu})\, d\sigma = \Phi\left(W_{ij}, W_{ji}, \vec{\nu}_{ij}\right) \ , \qquad (9)$$

with :

$$\vec{\nu}_{ij} = \int_{\partial C_{ij}} \vec{\nu} d\sigma \ . \qquad (10)$$

in which the metrics is taken into account in the normal mean vector ; the upwinding is obtained by using Ph. Roe 's flux splitting [8], written in short :

$$\Phi_{ROE}(U,V,\vec{\nu}) = \mathcal{F}(U,\vec{\nu}) + \mathcal{F}\frac{(V,\vec{\nu})}{2} - \mid \mathcal{R}(U,V,\vec{\nu}) \mid \frac{(V-U)}{2}, \qquad (11)$$

to complete the description of the scheme, W_{ij} and W_{ji} will be defined through interpolation involving "limited slopes" [3] which provide the basic

first-order accurate upwind scheme ($W_{ij} = W_i$ and $W_{ji} = W_j$) where extrema are detected.

Solution algorithm

In this presentation the choice of the resolution algorithm will not be discussed since we focus on the accuracy point of view.

In short, the algorithm [4] is an pseudo-unsteady one with local time stepping. The time-stepping is a linearised unfactored implicit one with Jacobi linear iteration. Time steps are increased in function of the inverse of the residual for better convergence, as in the SER method of Mulder and van Leer [7].

2. MESH ADAPTION

Mesh Criterion

The above scheme is considered as a perturbation of a central differenced one obtained by using, instead of ROE's flux splitting, the following function :

$$\Phi_C\,(U,V,\vec{\nu}) = \mathcal{F}\left(\frac{U+V}{2},\vec{\nu}\right) \tag{12}$$

then the following numerical viscosity estimate is considered :

$$E_{ij} = ||\Phi_{ROE}(W_{ij},W_{ji},\vec{\nu}_{ij}) - \Phi_C(W_i,W_j,\vec{\nu}_{ij})|| \tag{13}$$

where the norm is the Euclidean one.

Mesh Enrichment

One first way to locally adapt a mesh is to divide the elements of a well chosen region of the computational domain.

We can choose here between two options (see Figure 3) :

option (1) : we divide any segment ij for which E_{ij} is larger than a given parameter,

option (2) : in a smoother option, every triangle in which one at least side ij satisfies the above inequality is divided in four subtriangles.

Mesh Deformation System

In order to refine the mesh more efficiently in one direction (layers), we consider a mesh deformation method, relying on a spring analogy. The TVD criterion E_{ij} is introduced in the strength of each attraction spring between vertices i and j.

The mesh iteration is applied in alternation with the flow solution as sketched in the following algorithm :

(i) initialize mesh and flow
(ii) solve partially the flow
(iii) if the mesh is adapted enough, stop, else go to (iv)
(iv) compute E_{ij} and the strength of each spring
(v) solve partially the mesh system with fixed spring-strengths
(vi) transfer the flow on the new mesh
(vii) go to step (ii)

Step (vi) was rather unefficient since no consistent transfer such as in the ALE algorithm used in [6] ; we restricted to small displacements and to a few iterations of the above algorithm (3 to 10) ; since the flow solution is only partially converged, the cost of the total calculation is generally twice as costly as a non-adapted calculation.

3. NUMERICAL EXPERIMENTS

Capture of shocks

A numerical shock profiles generally consists in one region B with high gradient but more or less linear behaviour between two regions A and C with less high gradients, higher further derivatives and likely the arising of extremas. In most TVD schemes, the behaviour of the TVD sensor will in short produce first-order accuracy in region A and C and second-order accuracy in region B. With a TVD scheme that is central central-differenced for the second-accurate component, this may result in a small numerical viscosity in region B, and therefore unfortunately, in no refinement of this central zone of the shock.

Conversely, when using a MUSCL-TVD formulation, the second-order accurate component carries a numerical viscosity (third-order derivatives that bring a fourth-order error) that can be still large in region B, mainly because

fourth-order derivatives are computed on larger molecules while region B has only a one to three elements width ; we shall illustrate this point in the experiments below.

Euler flow around a NACA0012 airfoil

As example of mesh enrichment based on the criterion (13), we compute an Euler flow .The farfield Mach number is equal to .85.The angle of attack is 0. The uniform initial mesh (800 vertices) is enriched once (Figure 4). In spite of the low numberof nodes in the final mesh (1717 vertices), we observ a better capture of the shock (Figure 5).

Navier-Stokes flow past a flat plate

For a demonstration of the basic qualities of the method we consider the flow past a plate at Reynolds number 1000 and Mach number at farfield 3.

An uniform initial mesh (1138 vertices) is enriched twice using the TVD criterion, resulting in a 6480-vertices mesh (Figure 6), and then deformed using the same criterion (Figure 7).

While an intuitive idea of the overall improvement is given by several contours (Figs. 8 and 9), the more striking comparison is related to the friction coefficient (Figs. 10 and 11).

Flow around a NACA0012 airfoil

We consider a more complex flow around a NACA0012 airfoil, with farfield Mach number of 2 an angle of attack of 10 degrees and a Reynolds number of 1000. This case was proposed in a workshop [10] in 1985. A very thin detached shock is present. The starting uniform mesh (Figs. 12 to 15) is enriched 3 times (Figs. 16 to 27). The same strategy (enrichment and then deformation) is applied. The final mesh contains 7926 nodes (Figs. 28 and 30). We present the corresponding Mach contours (Figs. 29 and 31) : some extra refinement seems needed for a thin capture of the shock ; the boundary layer is rather well computed.

4. CONCLUDING REMARKS

The TVD criterion that we introduced is a rather general one. Some experiments with mesh local division shows its behavior in the contex of Euler and Navier-Stokes low Reynolds flows.

When combined with mesh deformation with springs, the TVD criterion proves to be rather smooth, except when only two or three rows of elements

are expect to capture a thin layer ; in this case the behavior is still satisfactory and no smoothing of the criterion is needed.

The challenge of high Reynolds with thin layers remains : more efficiency is needed for solving the coupling between flow and mesh.

REFERENCES

[1] Ph.M. GRESHO, R.L. LEE, Dont' suppress the wiggles. They are telling you something !, in Finite Element methods for Convection Dominated flows, New York, Dec. 2-7, 1979.

[2] L. FEZOUI, Résolution des équations d'Euler par un schéma de van Leer en éléments finis, INRIA Report 358, 1985.

[3] B. STOUFFLET, J. PERIAUX, L. FEZOUI, A. DERVIEUX, Numerical simulation of 3-D hypersonic Euler flows around space vehicles, 25th AIAA Conf., Reno, 1987, AIAA paper 87-0560.

[4] L. FEZOUI, S. LANTERI, B. LARROUTUROU,C. OLIVIER, Résolution numérique des équations de Navier-Stokes pour un fluide compressible en maillage triangulaire, INRIA Report, 1989.

[5] Ph. ROSTAND, B. STOUFFLET, Finite volume Galerkin methods for viscous gas dynamics, INRIA Report 863, 1988.

[6] B. PALMERIO, A. DERVIEUX, A 3-D unstructured-mesh adaption relying on physical analogy, Comm. to Numerical Grid Generation in Computational Fluid Mechanics, Miami, Dec. 1988.

[7] B. van LEER, W.A. MULDER, Relaxation methods for hyperbolic equations, in Numerical Methods for the Euler Equations of Fluid Dynamics, Angrand et al. Eds., SIAM (1985)

[8] Ph. L. ROE, Approximate Riemann solvers, parameters vectors and difference schemes, J. of Comp. Phys., 43, 357-371 (1981)

[9] V. BILLEY, A. DERVIEUX, L. FEZOUI, J. PERIAUX, V. SELMIN, B. STOUFFLET, Recent improvement in Galerkin and upwind Euler solvers and application to 3-D transonic flow in aircraft design, in Eighth Int. Conf. on Computer Methods in Applied Science and Engineering, Versailles, dec. 1987, North Holland 1988

[10] M. O. BRISTEAU, R. GLOWINSKI, J. PERIAUX, H. VIVIAND, (Eds) Numerical simulation of compressible Navier-Stokes flows, Note on Numerical Fluid Mechanics, 18, Vieweg, Braunschweig (1987)

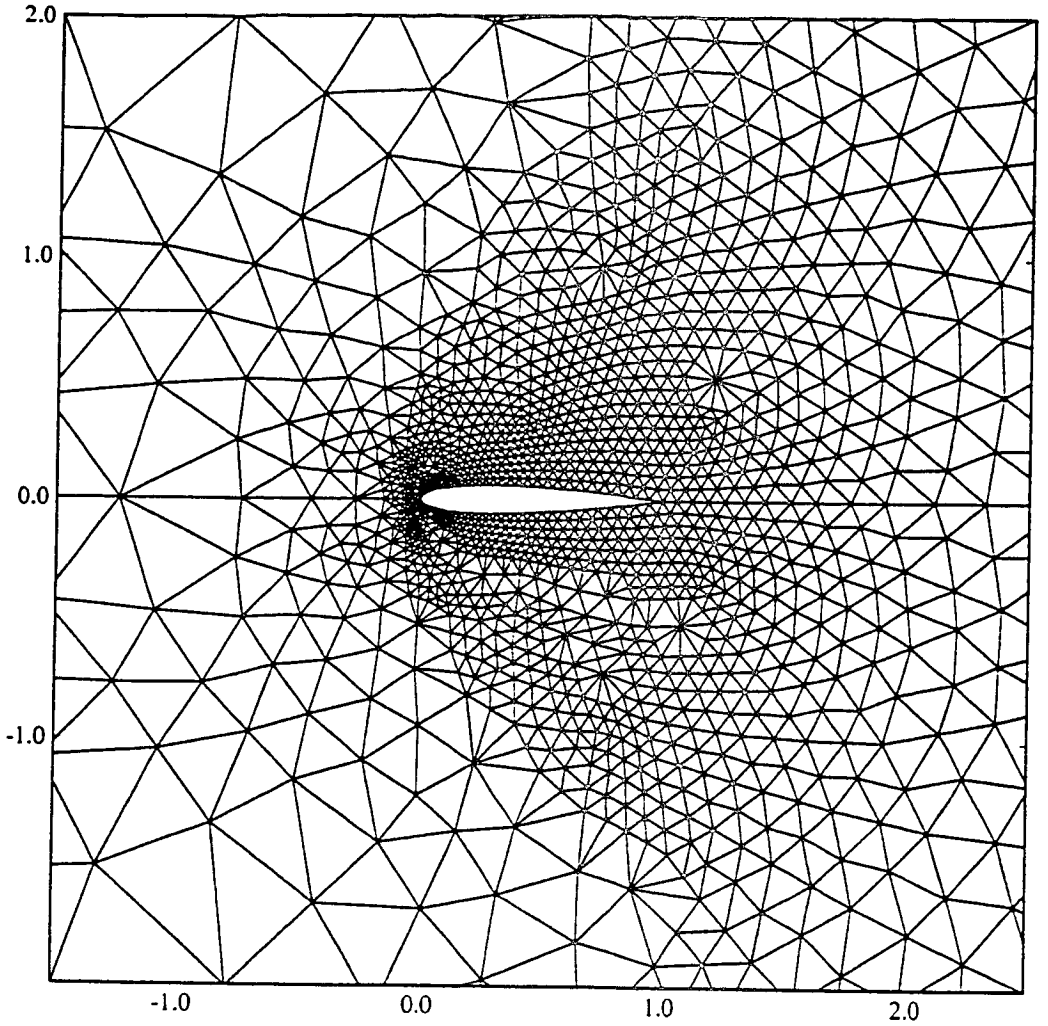

Figure 3 : Sketch of
options 1 and 2
NACA0012 airfoil
Mach=2
Reynolds=1000

Enriched mesh
option 1 (2071 nodes)

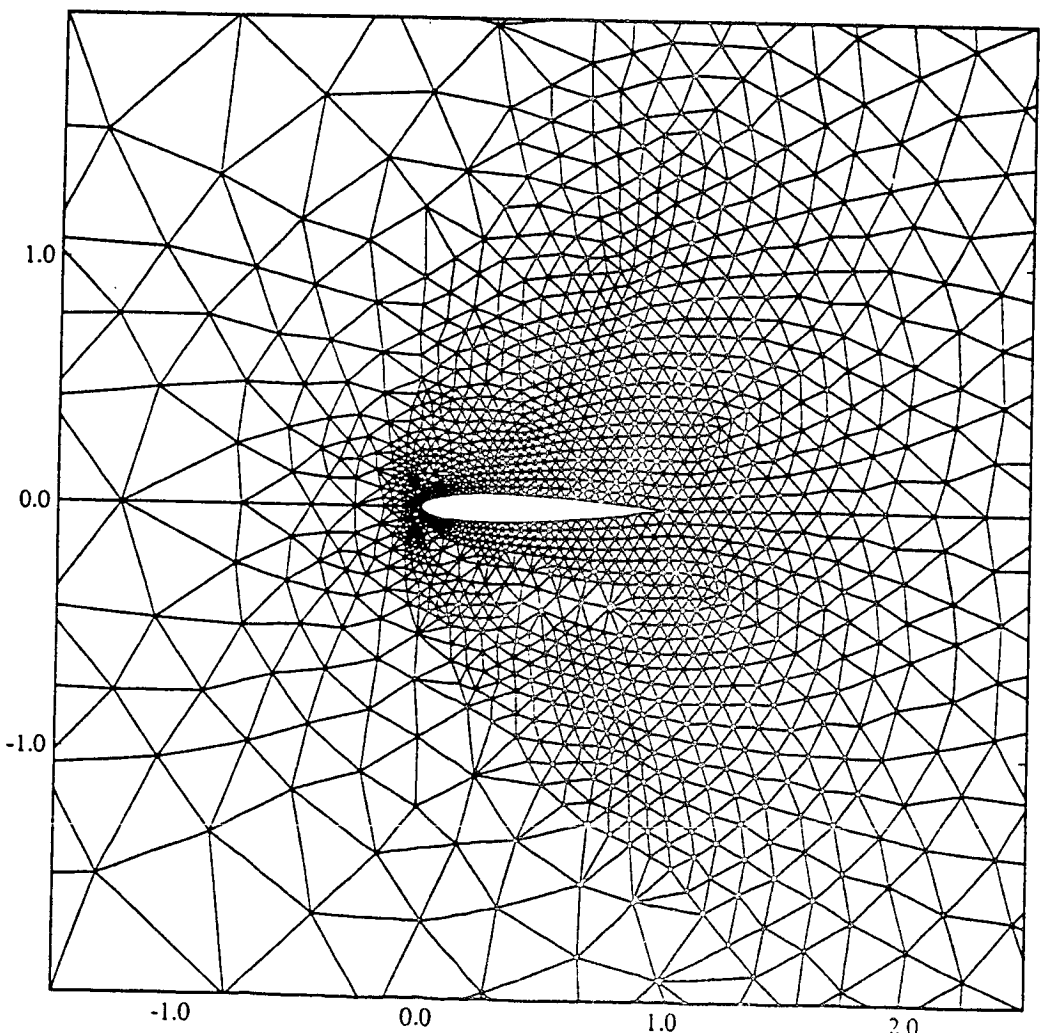

Enriched mesh
option 2 (2180 nodes)

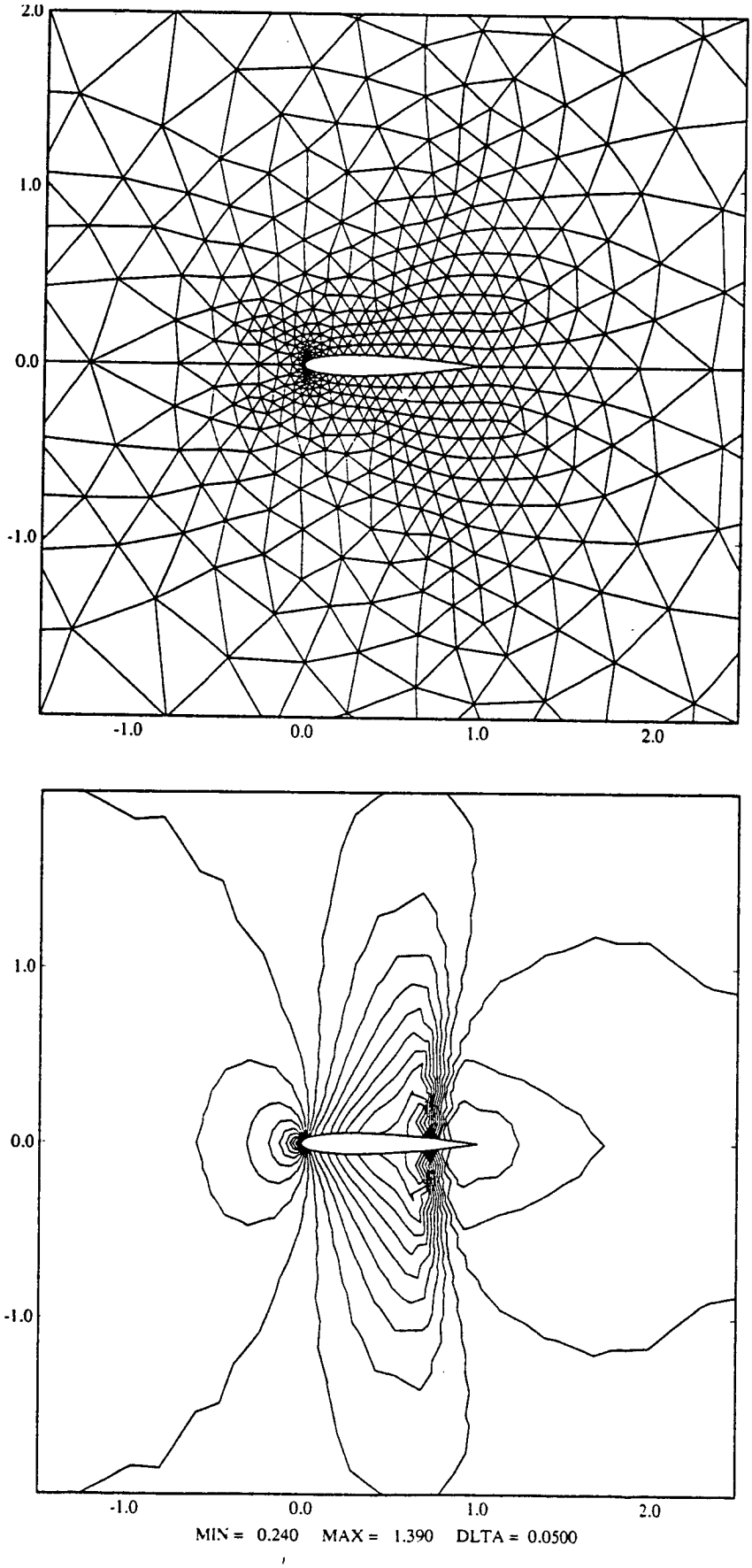

Figure 4 : Euler flow past a NACA0012 airfoil, Mach = .85
Initial mesh (800 nodes) and corresponding Mach contours

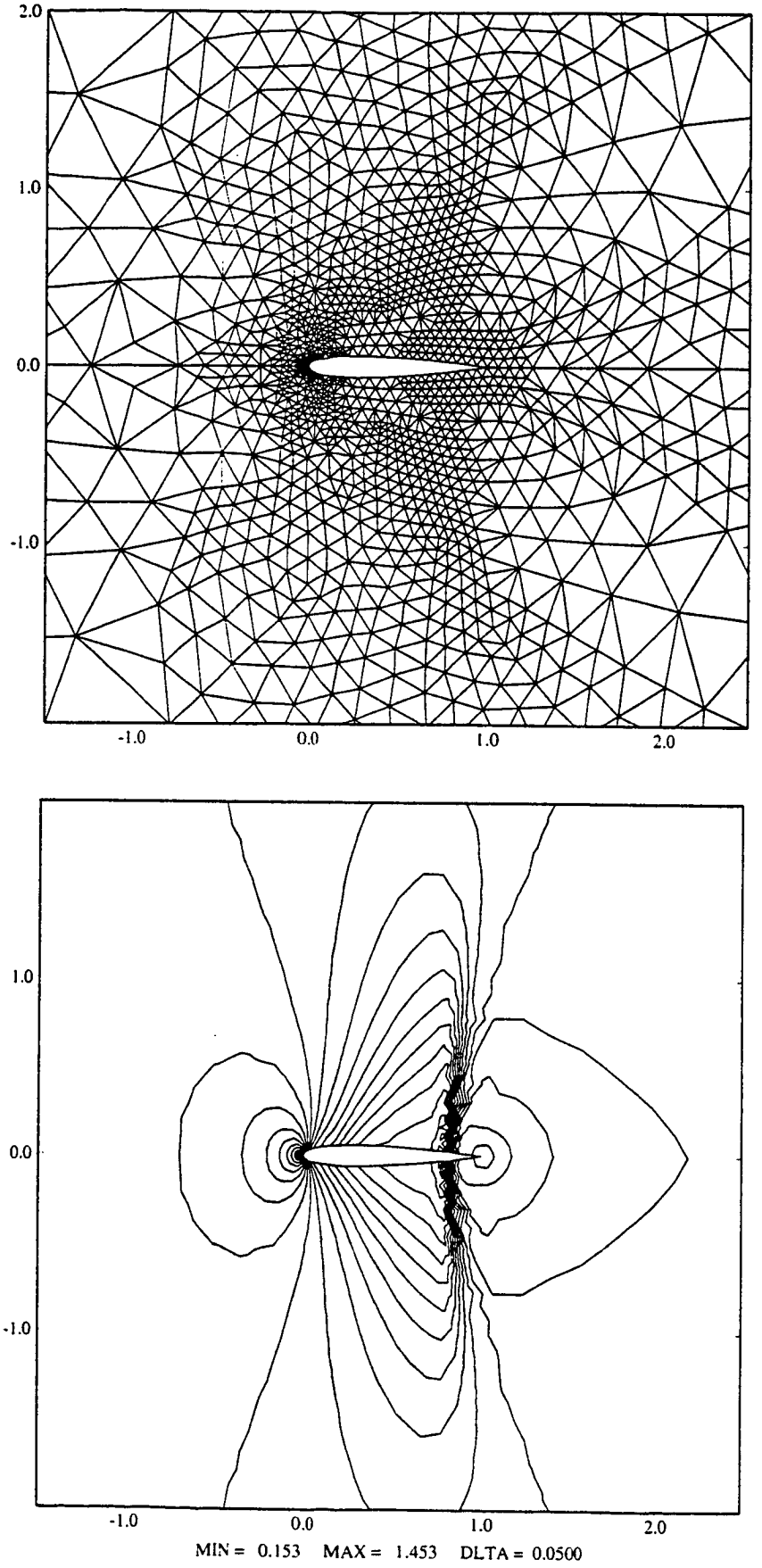

Figure 5 : Euler flow past a NACA0012 airfoil, Mach = .85
Enriched mesh (1717 nodes) and corresponding Mach contours

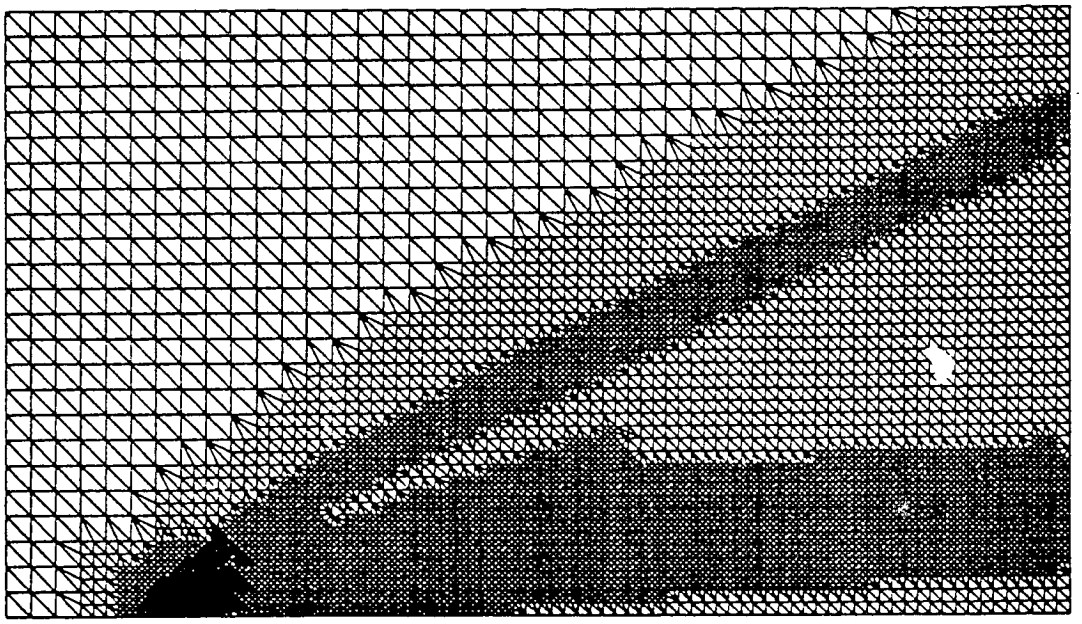

Figure 6 : Enriched mesh for the plate problem

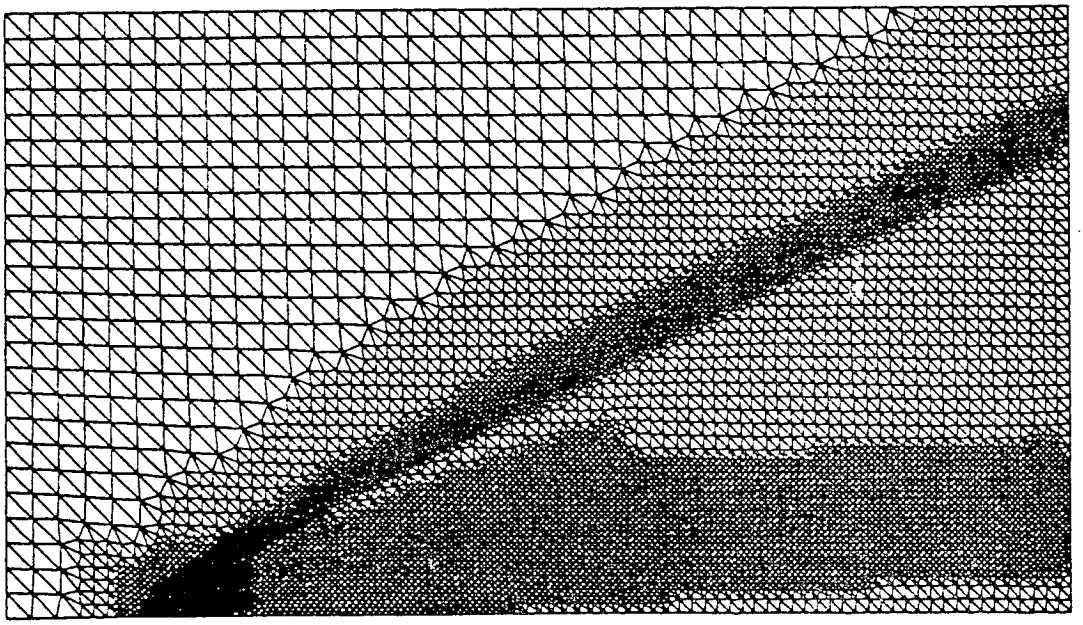

Figure 7 : Enriched and deformed mesh for the plate problem

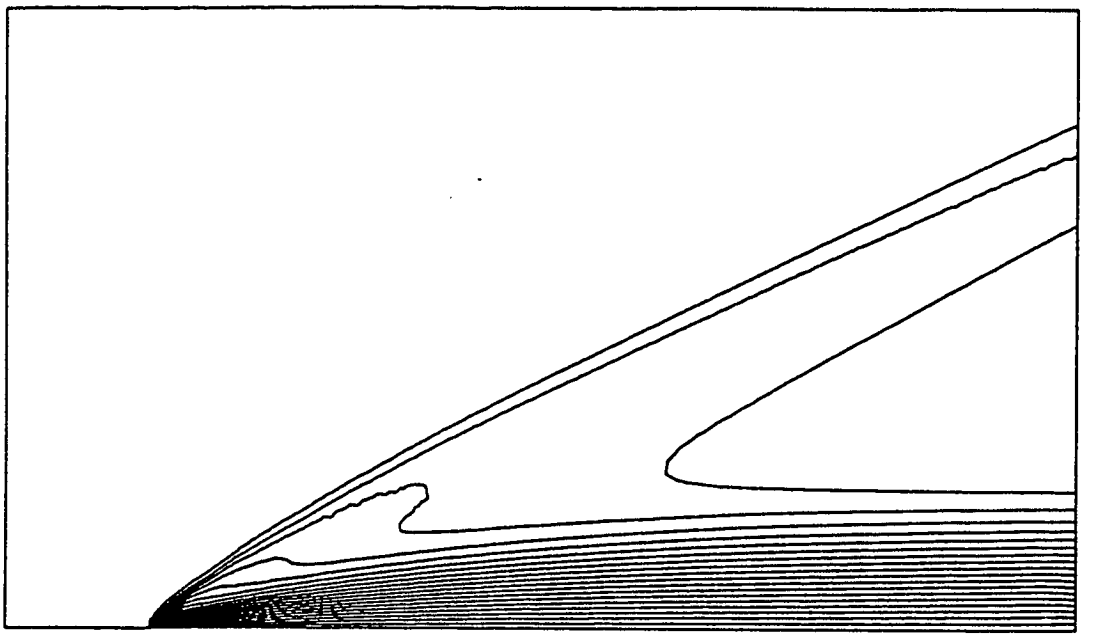

Figure 8 : Mach contours with the enriched mesh

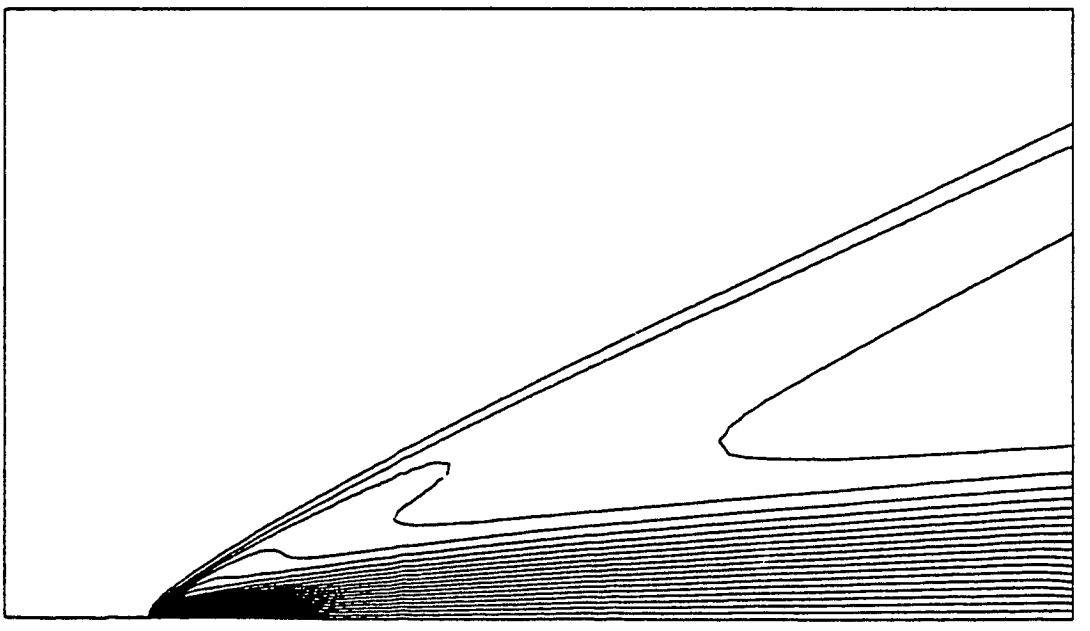

Figure 9 : Mach contours for the enriched and deformed mesh

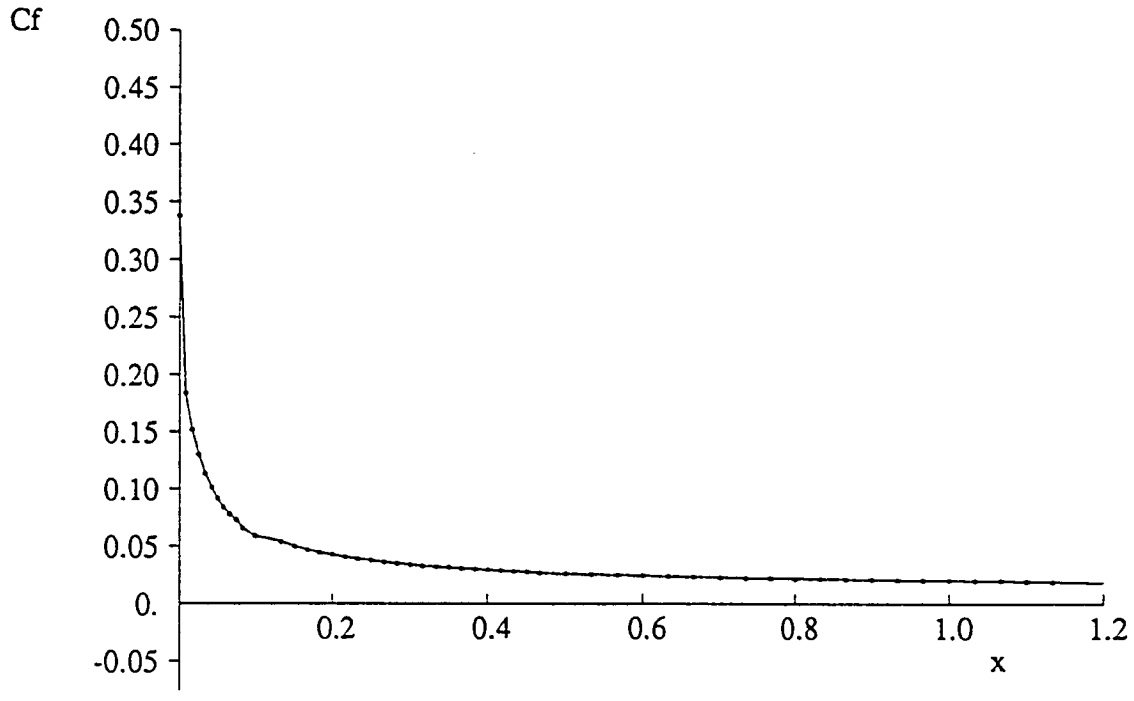

Figure 10 : Friction coefficient with the enriched mesh

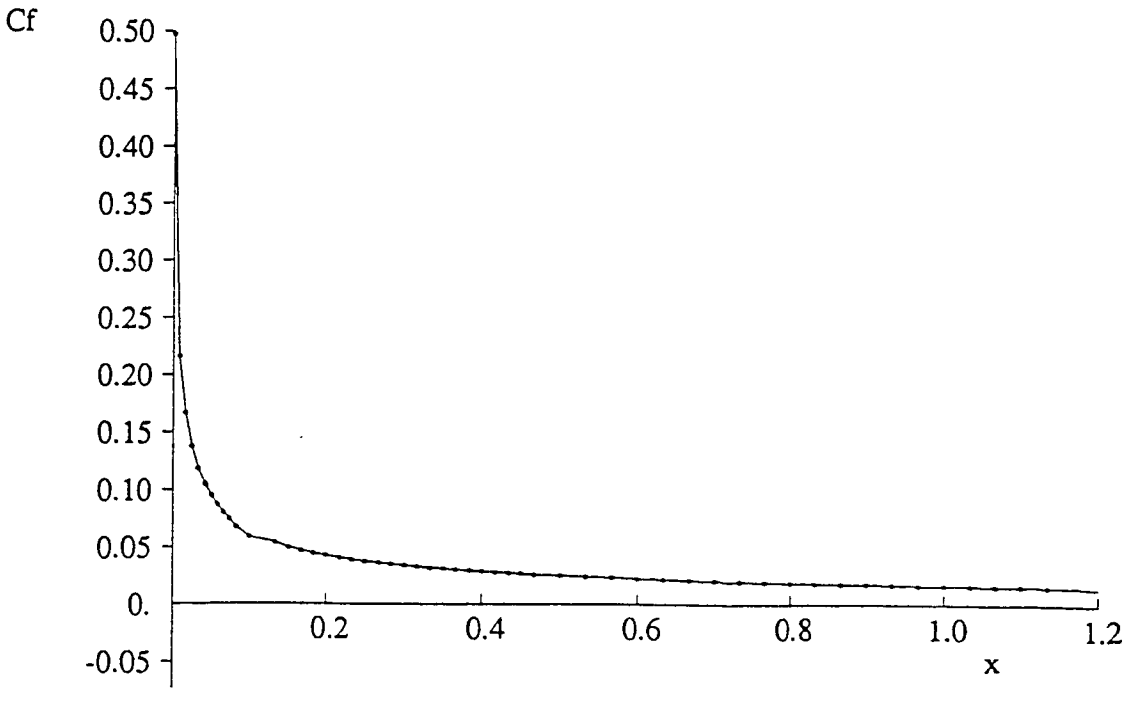

Figure 11 : Friction Coefficient for the enriched and deformed mesh

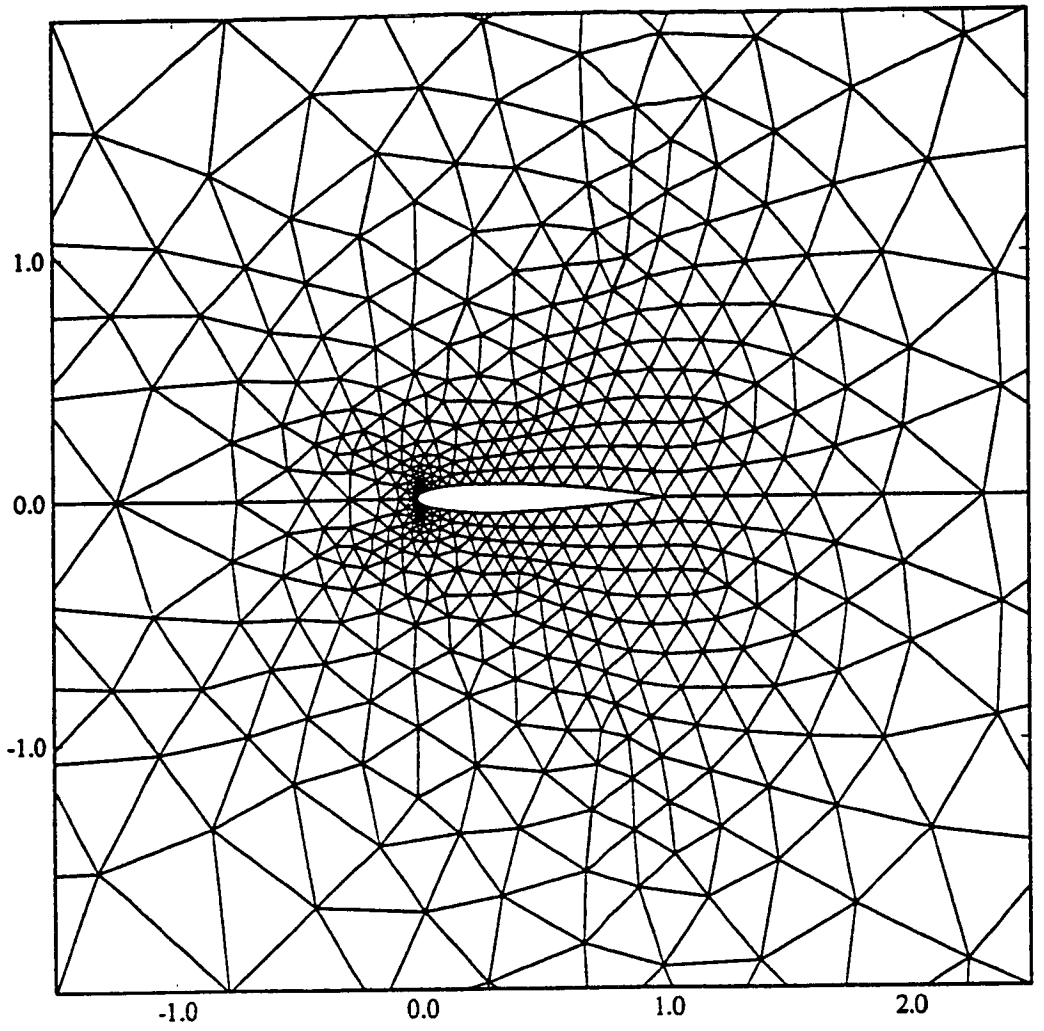

Figure 12 :
NACA0012 airfoil
Mach=2
Reynolds=1000
Initial mesh (800 nodes)

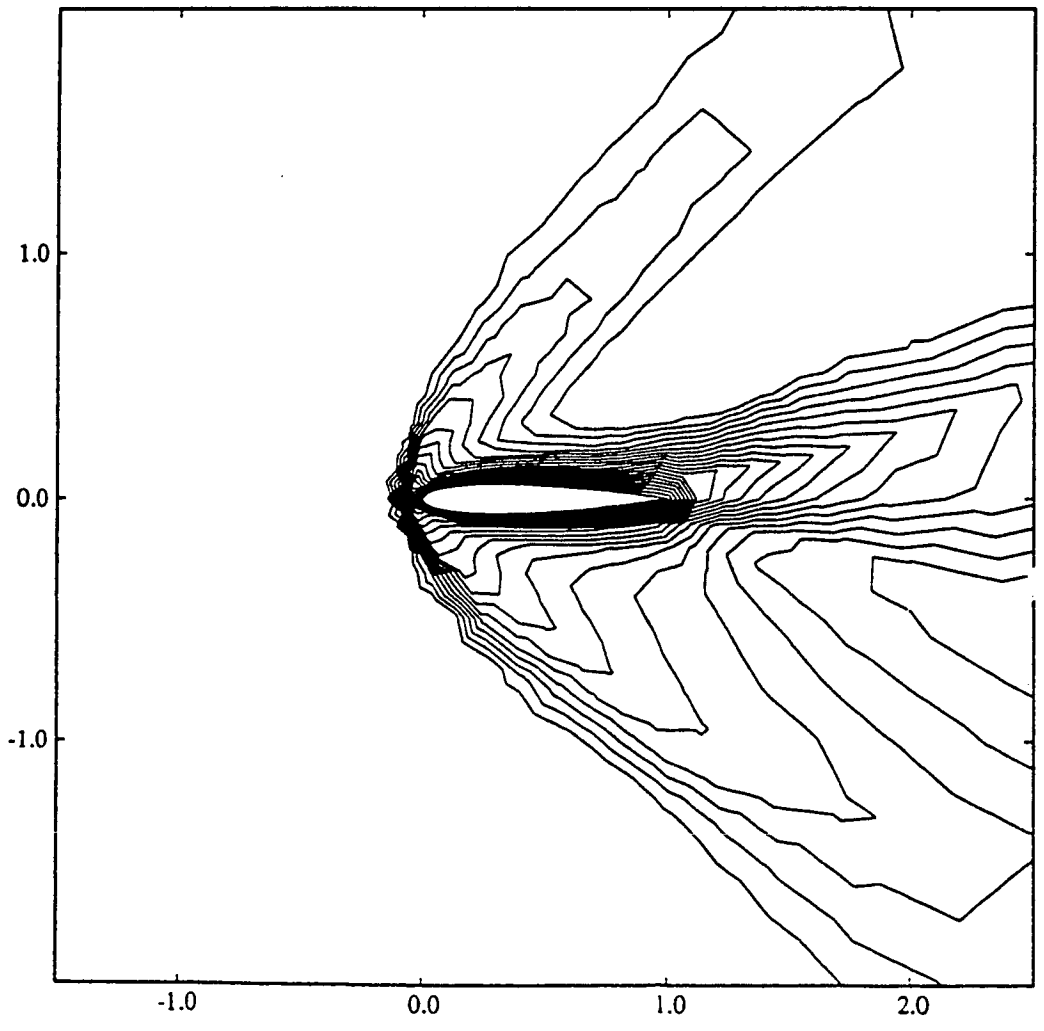

Figure 13 :
Corresponding
Mach contours

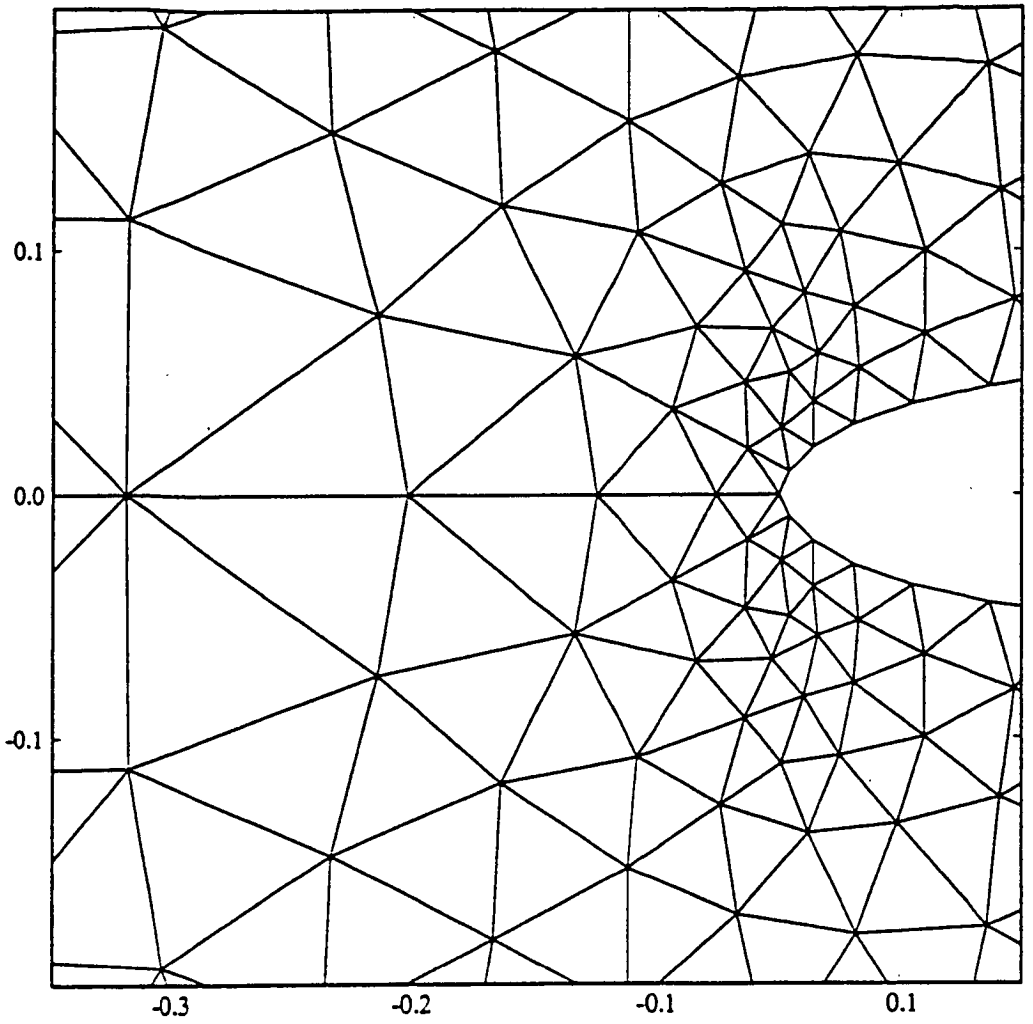

Figure 14 :
Partial view
of the Fig. 12

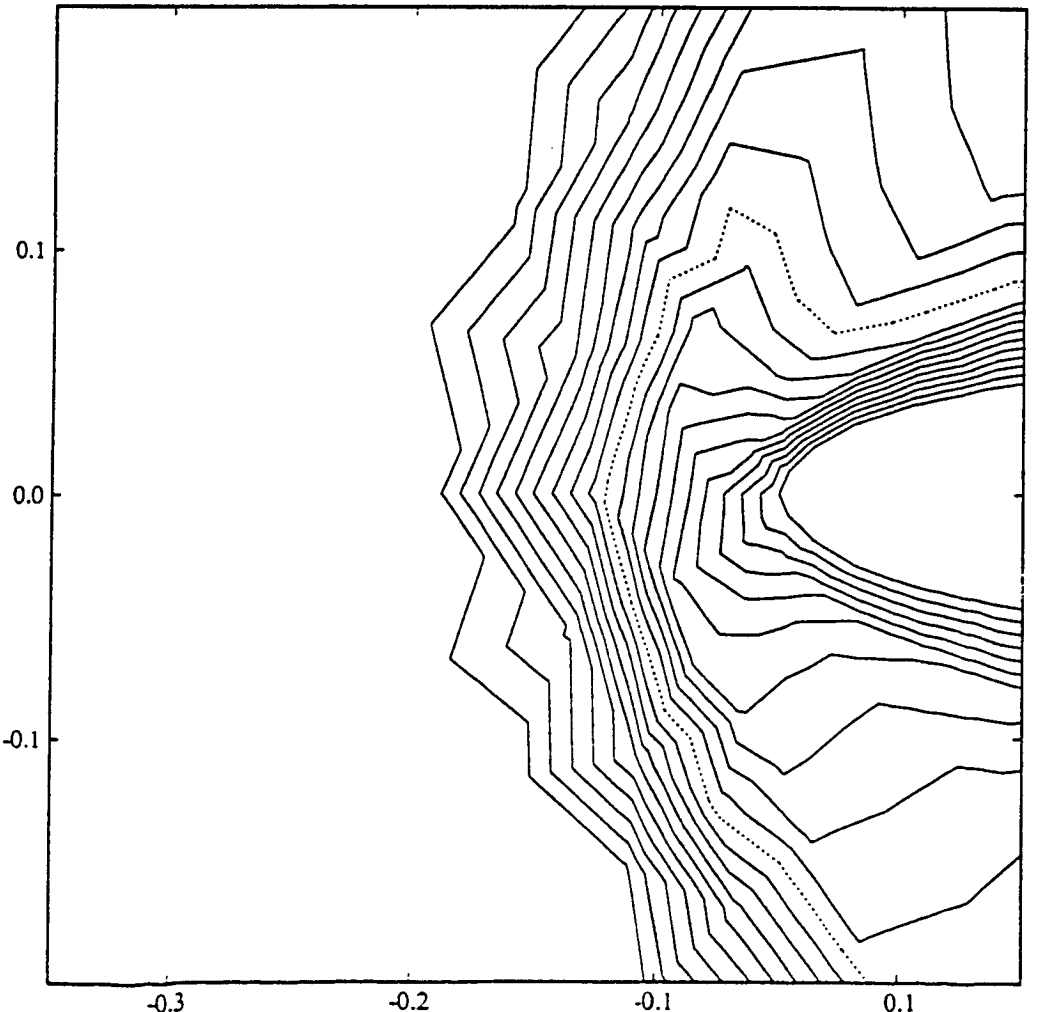

Figure 15 :
Partial view
of the Fig. 13

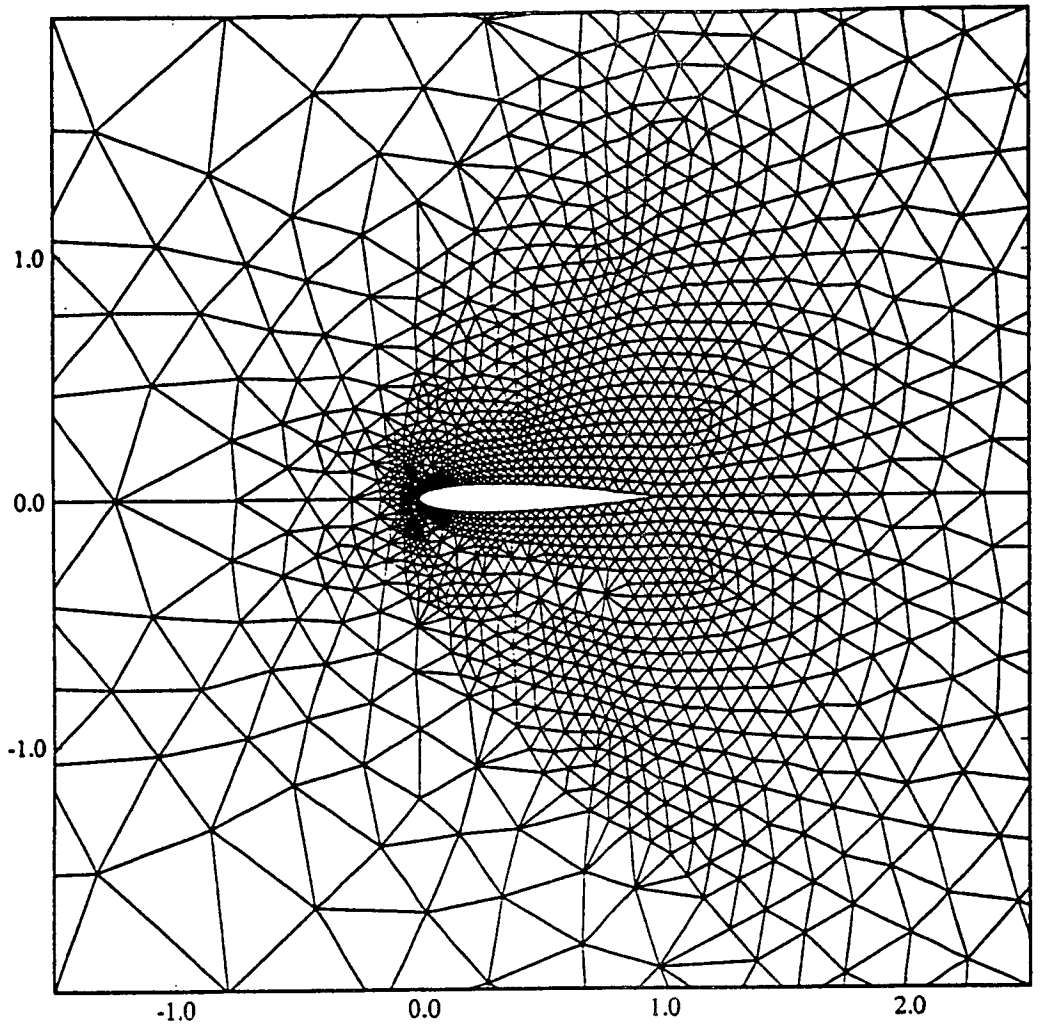

Figure 16 :
NACA0012 airfoil
Mach=2
Reynolds=1000
First enriched mesh
(2005 nodes)

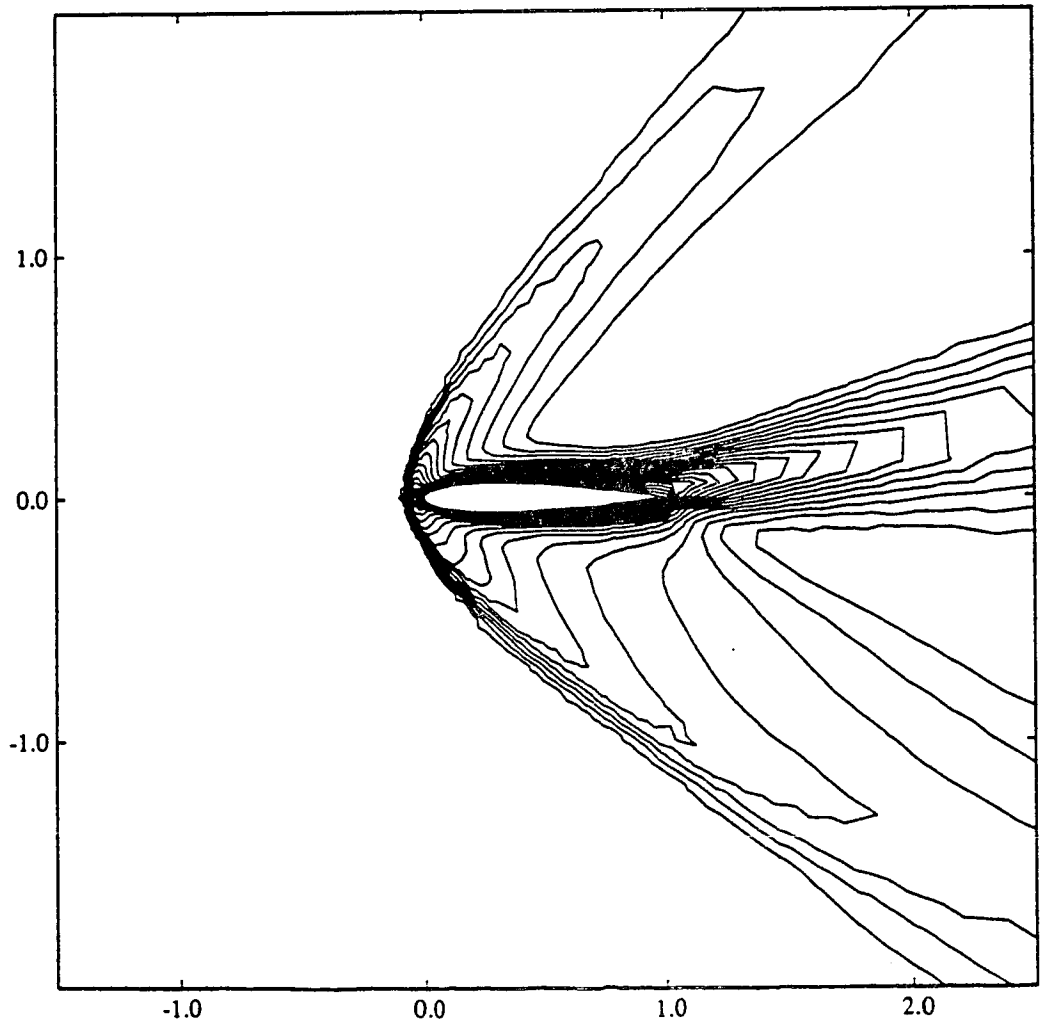

Figure 17 :
Corresponding
Mach contours

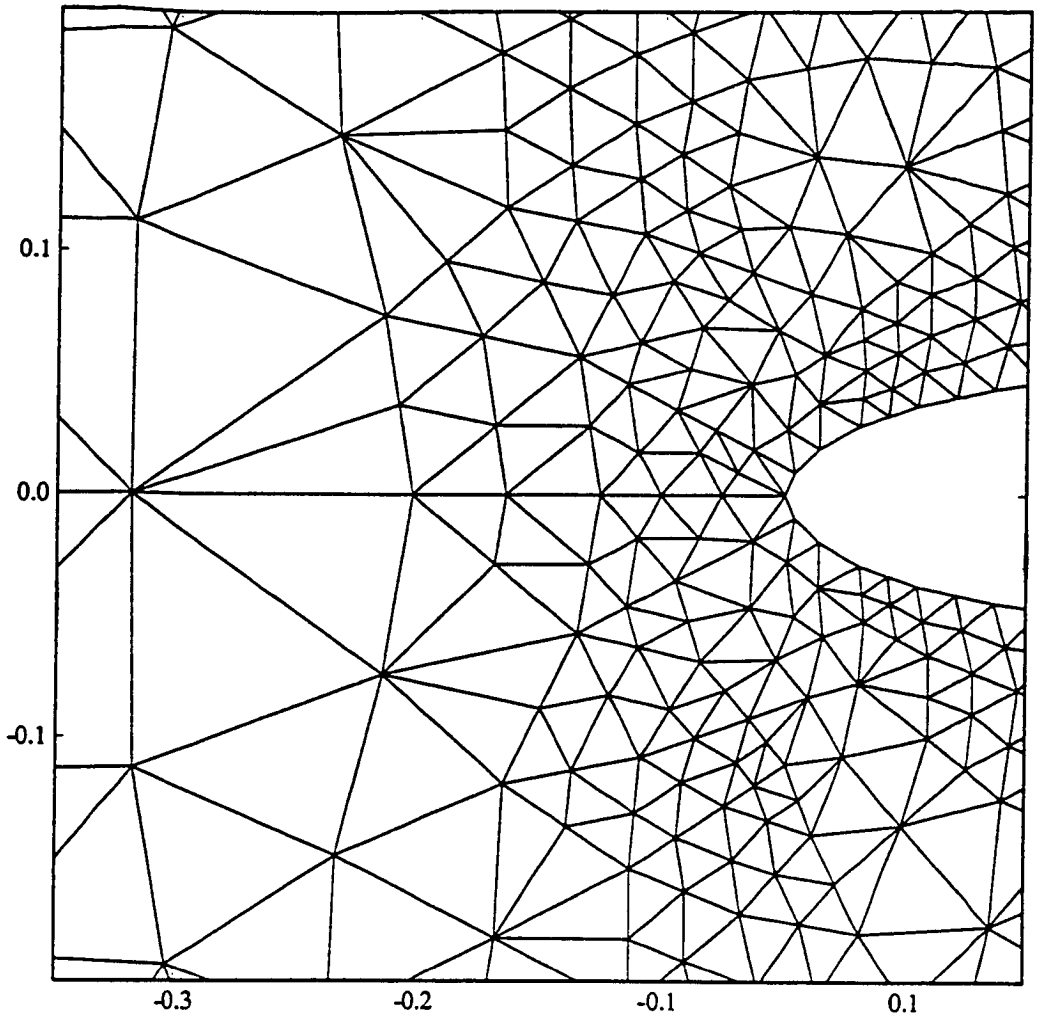

Figure 18 :
Partial view
of the Fig. 16

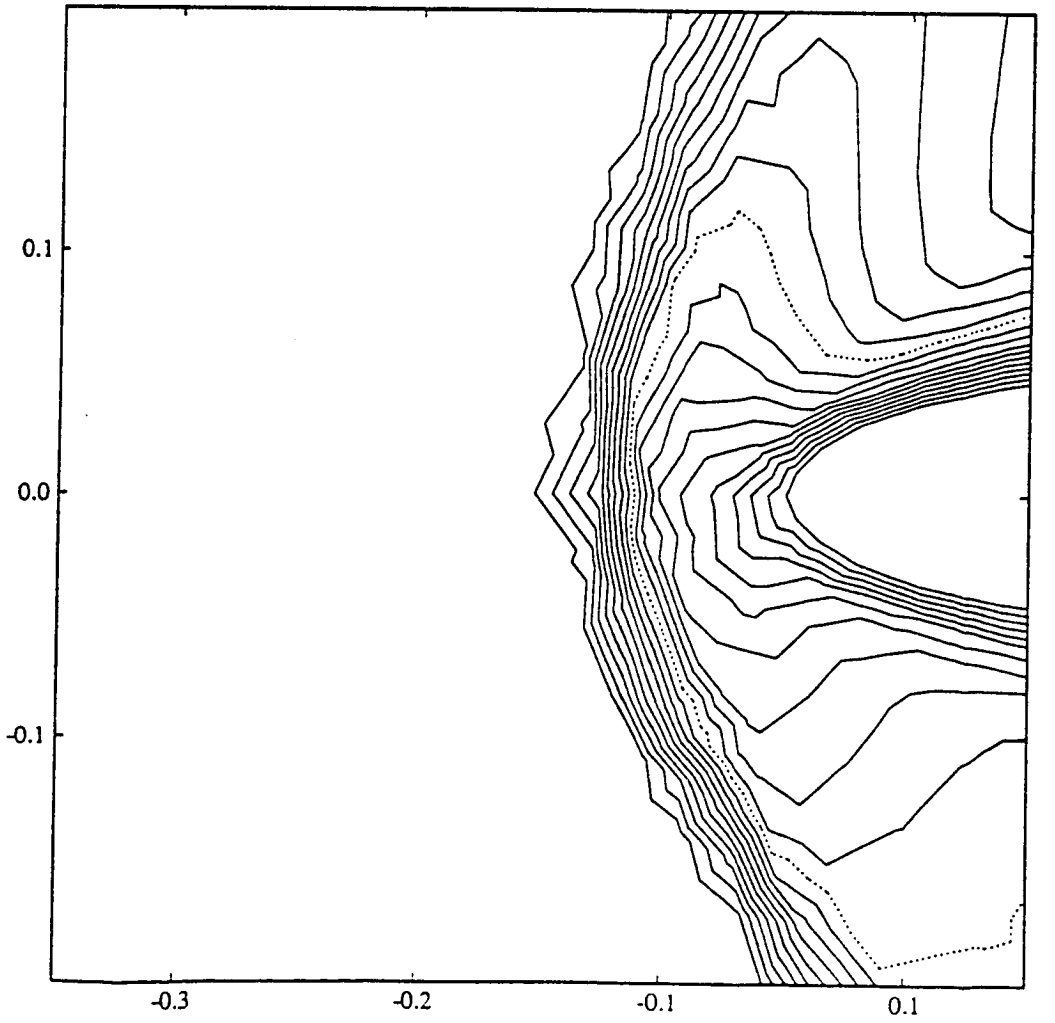

Figure 19 :
Partial view
of the Fig. 17

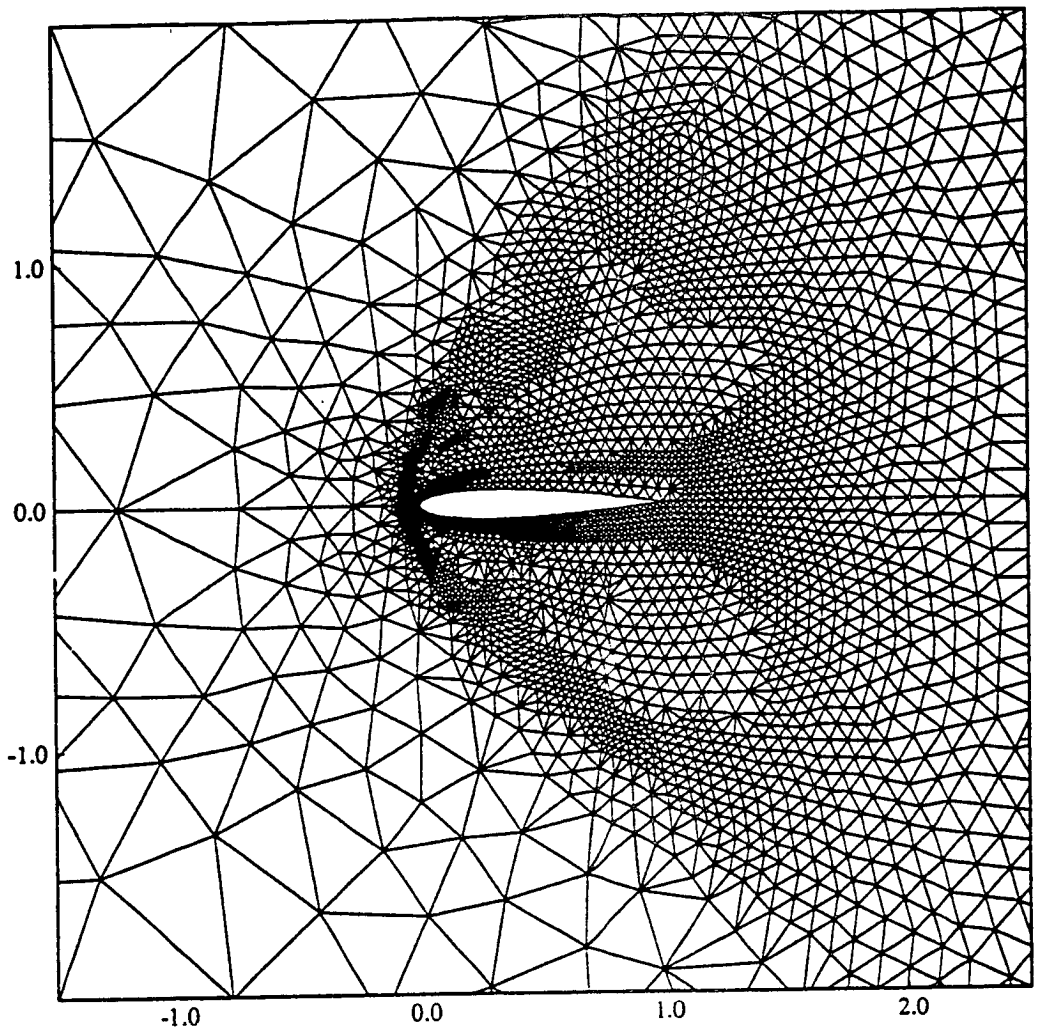

Figure 20 :
NACA0012 airfoil
Mach=2
Reynolds=1000
Twice enriched mesh
(4960 nodes)

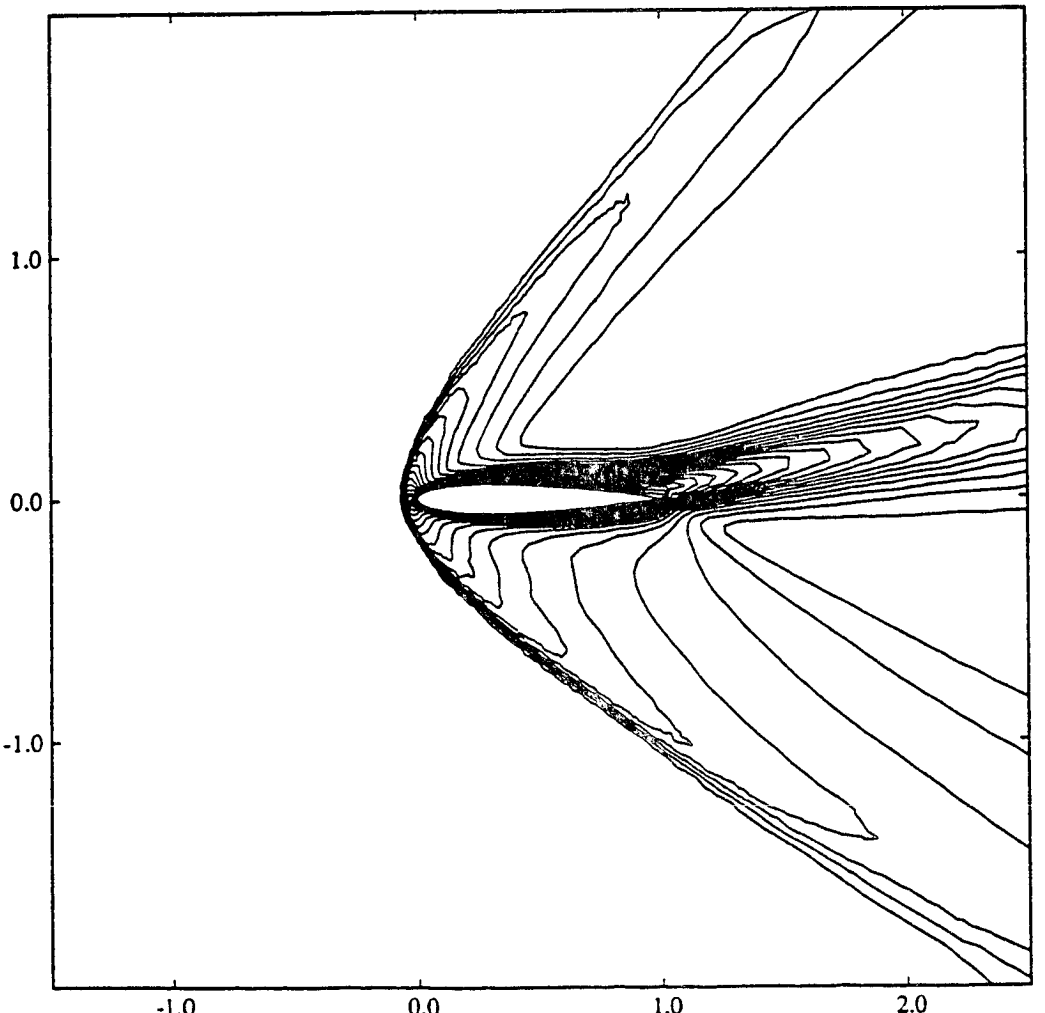

Figure 21 :
Corresponding
Mach contours

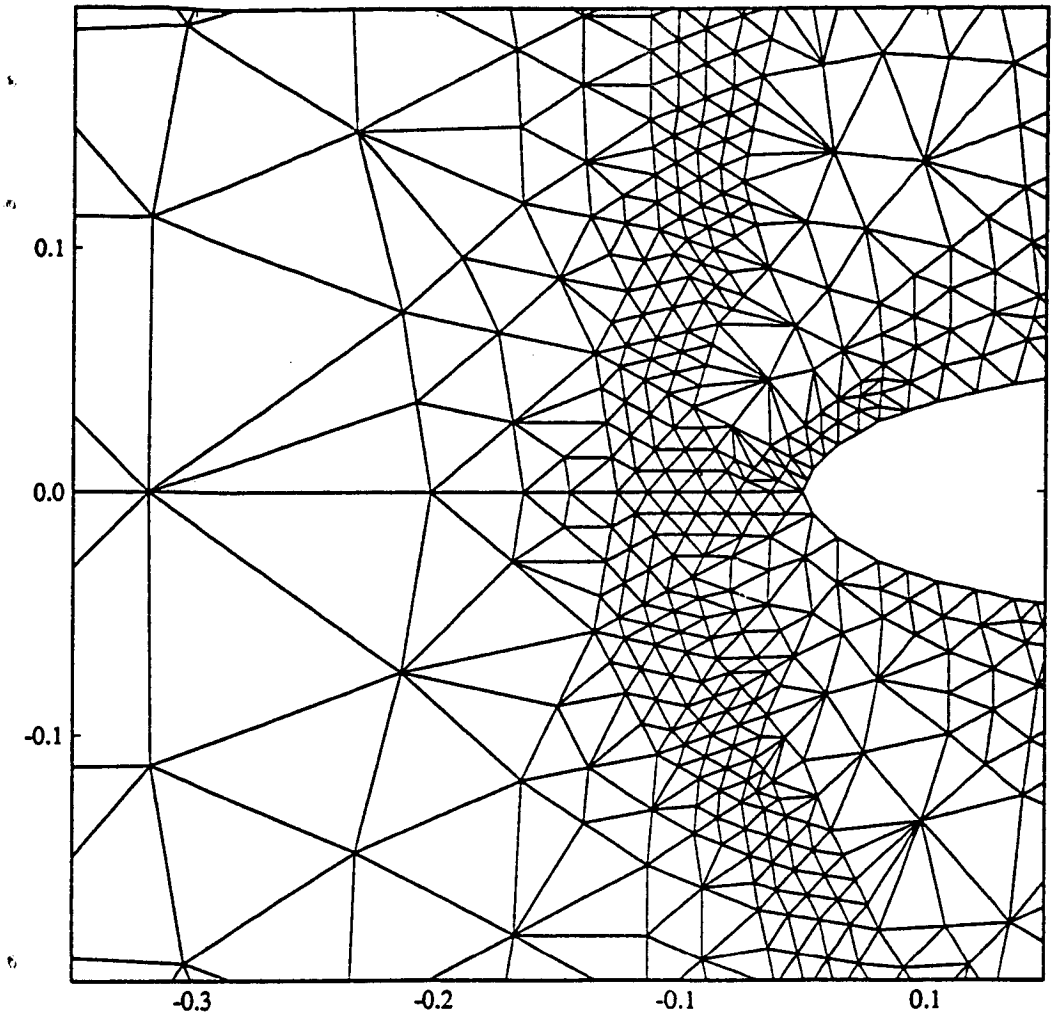

Figure 22 :
Partial view
of Fig. 20

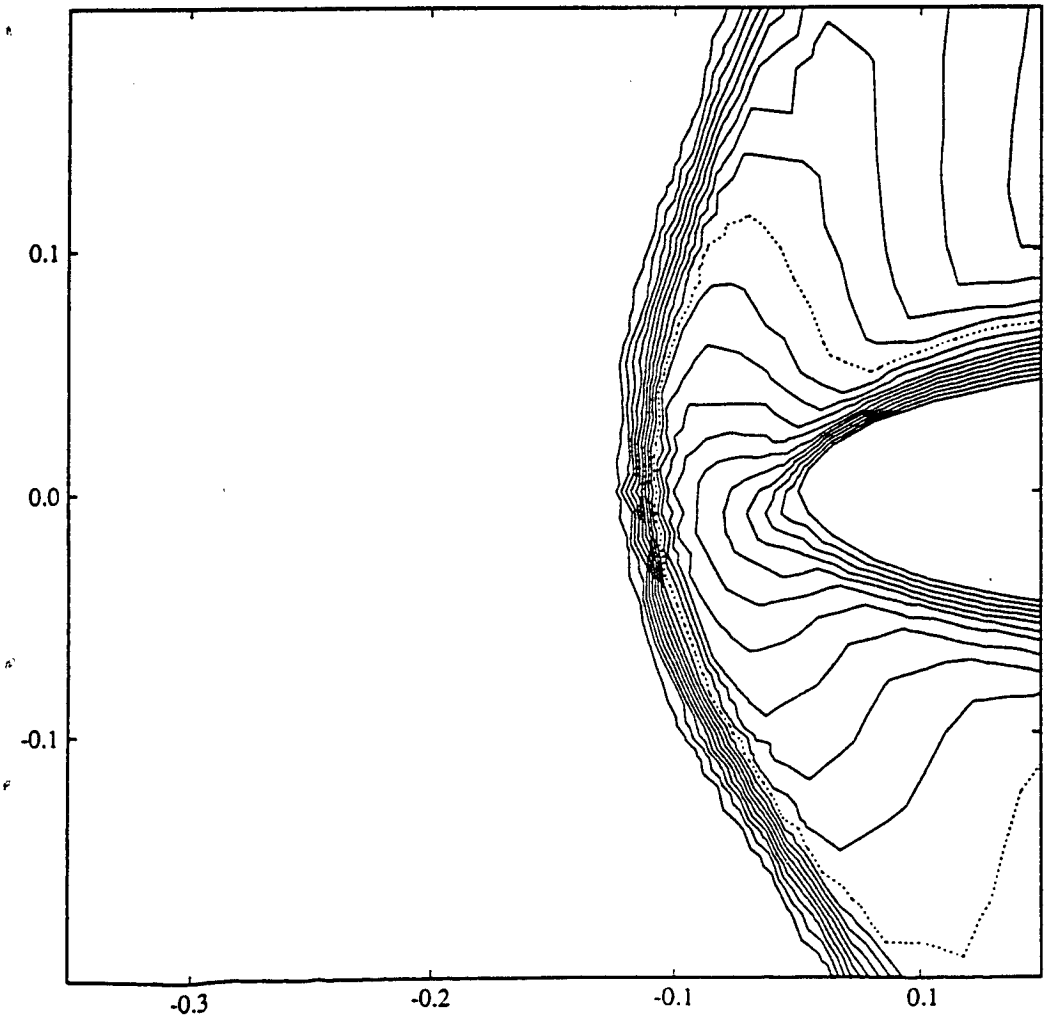

Figure 23 :
Partial view
of Fig. 21

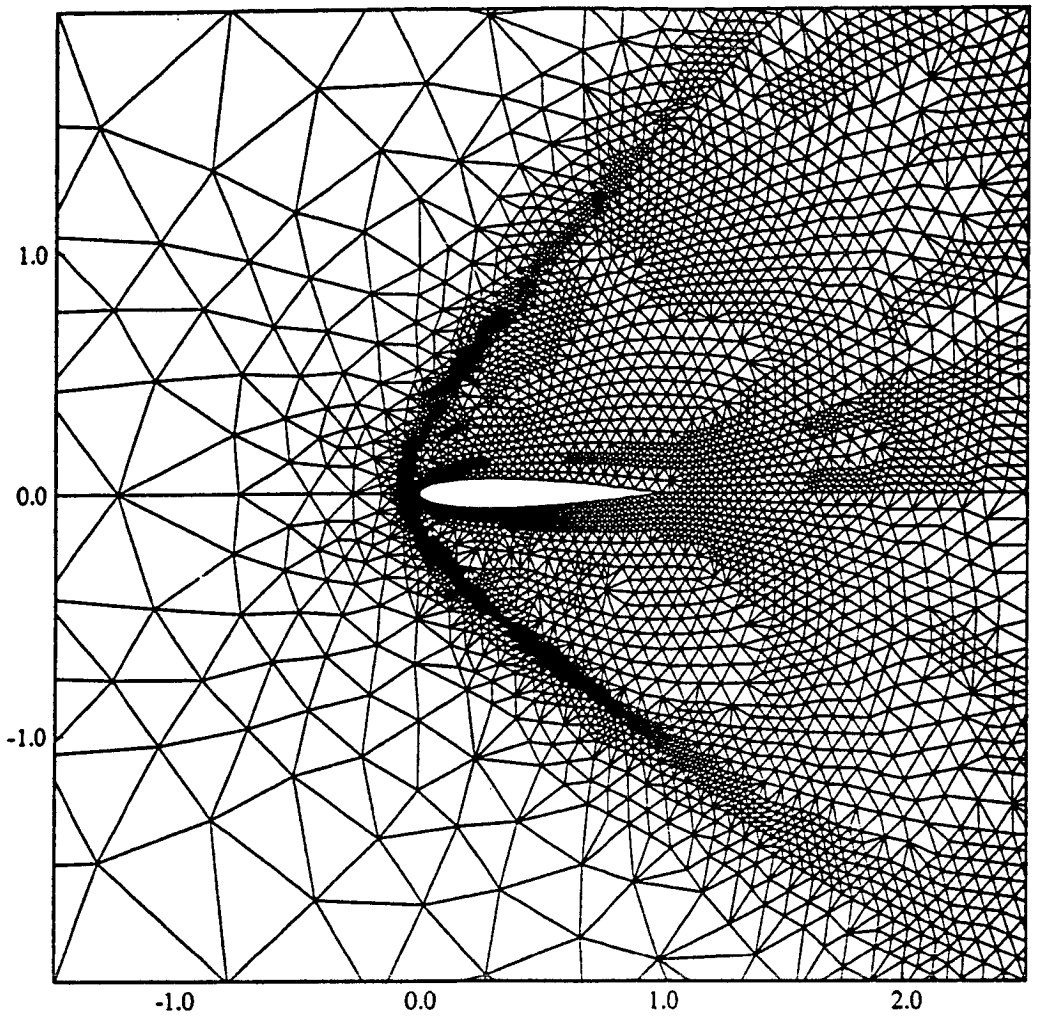

Figure 24 :
NACA0012 airfoil
Mach=2
Reynolds=1000
3 times enriched mesh
(7926 nodes)

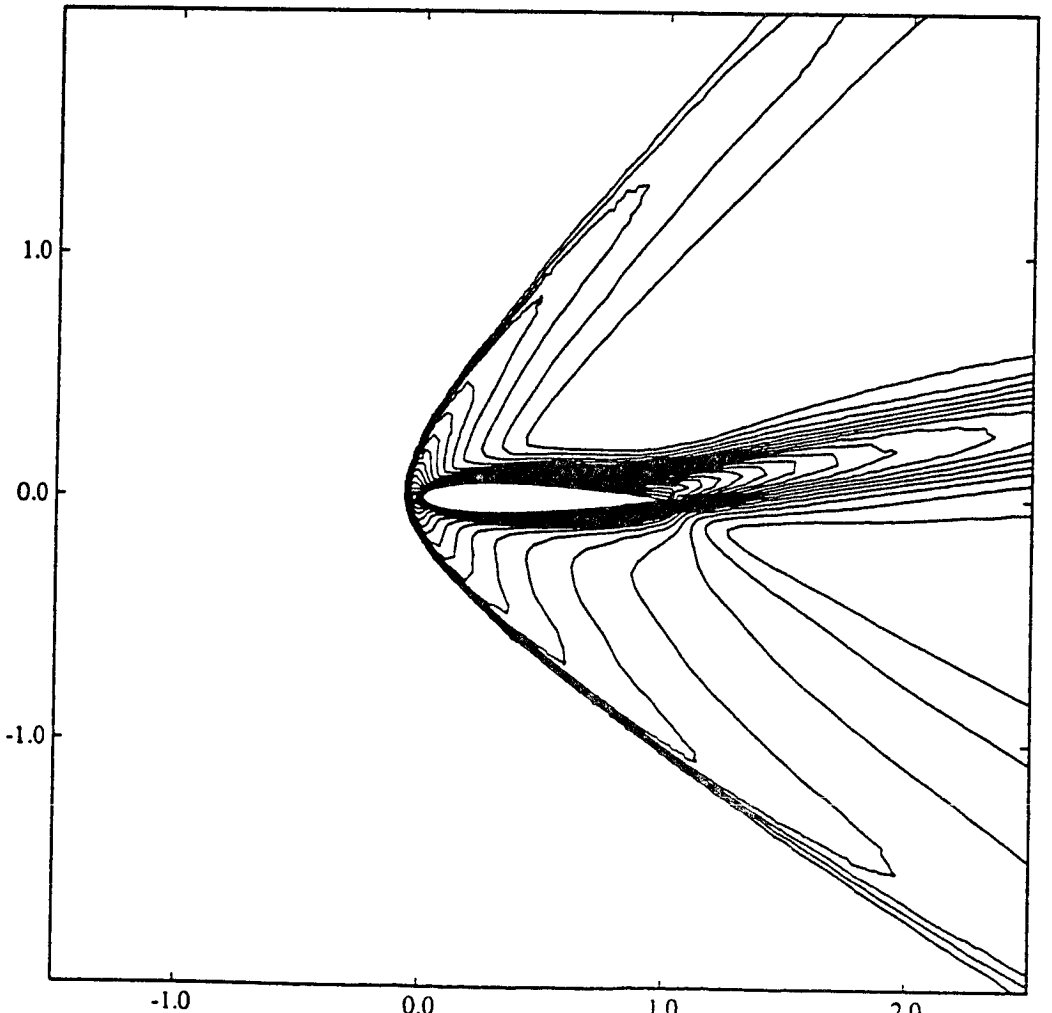

Figure 25 :
Corresponding
Mach contours

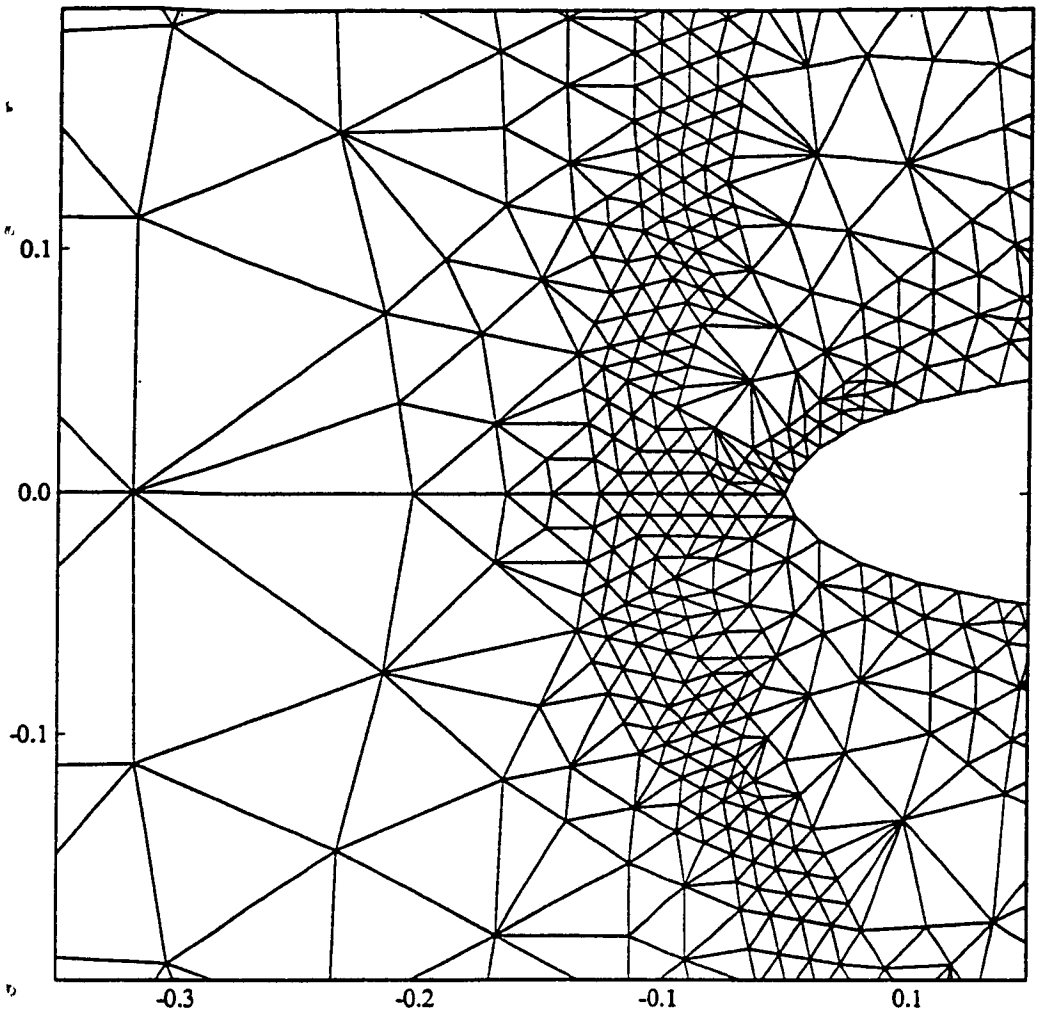

Figure 26 :
Partial view
of F g. 24

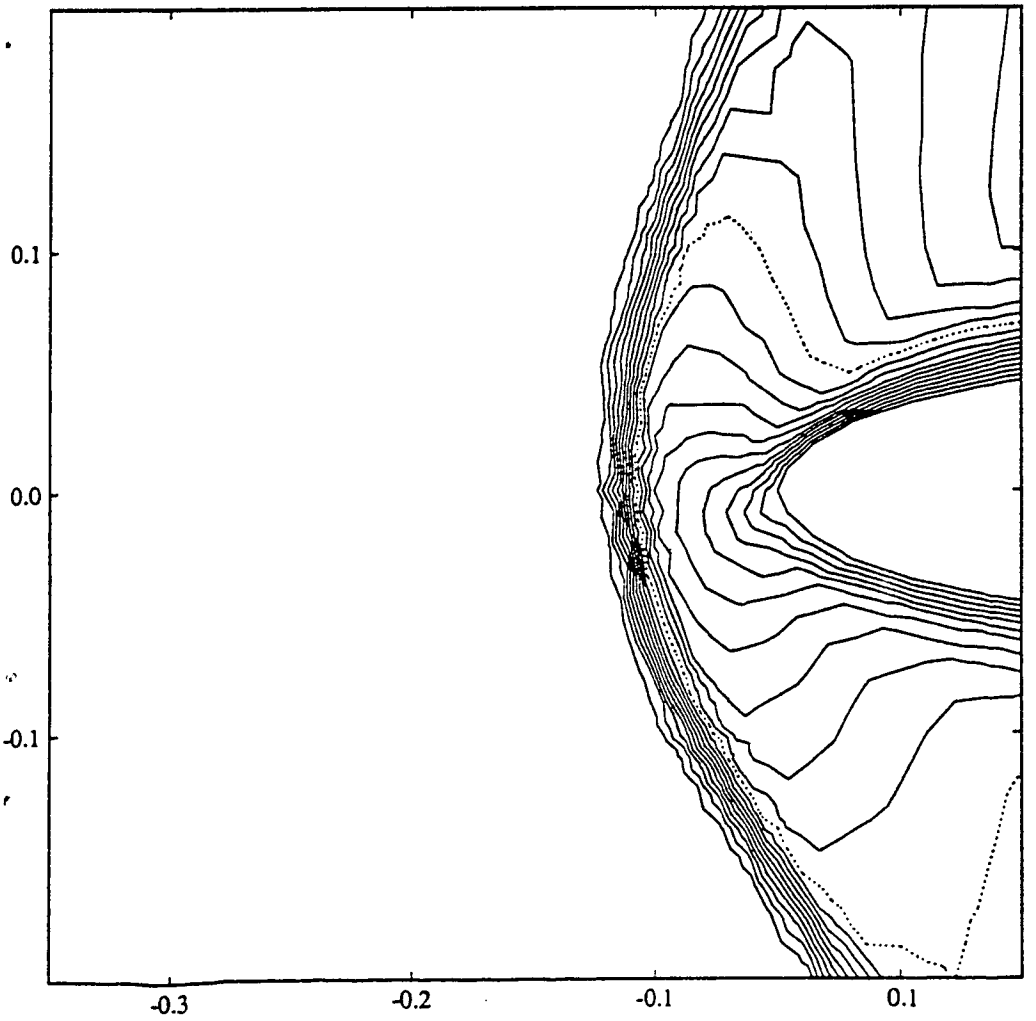

Figure 27 :
Partial view
of the Fig. 25

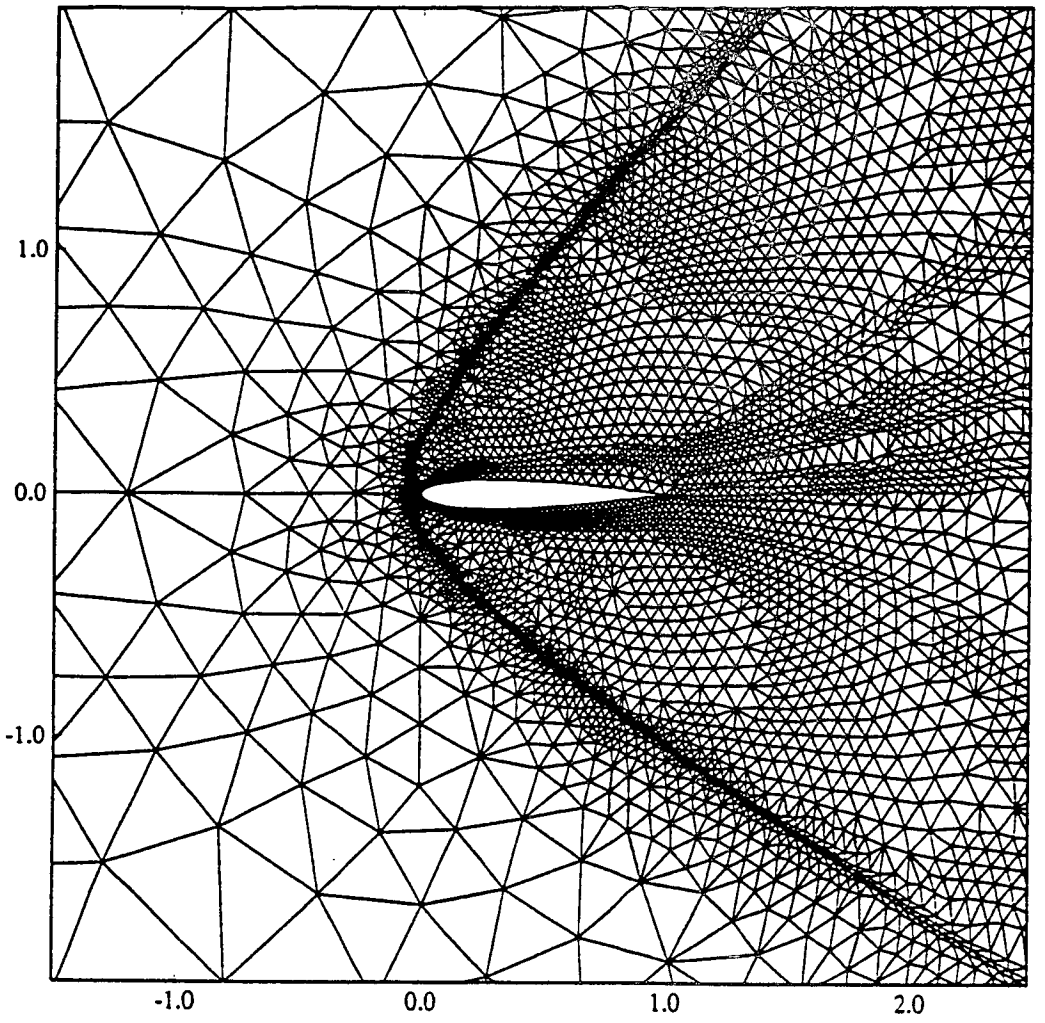

Figure 28 :
NACA0012 airfoil
Mach=2
Reynolds=1000
Final mesh
(7?26 nodes)

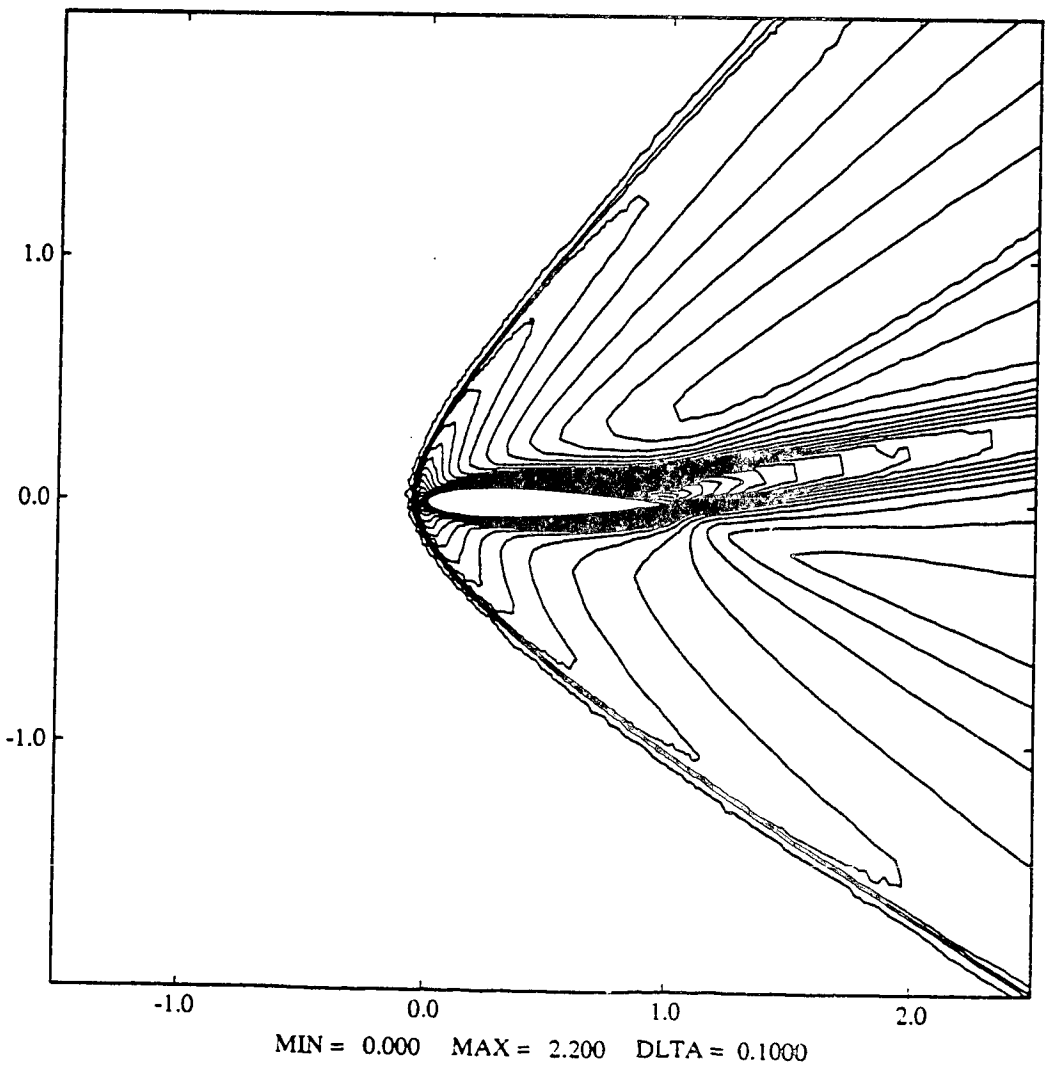

Figure 29 :
Corresponding
Mach contours

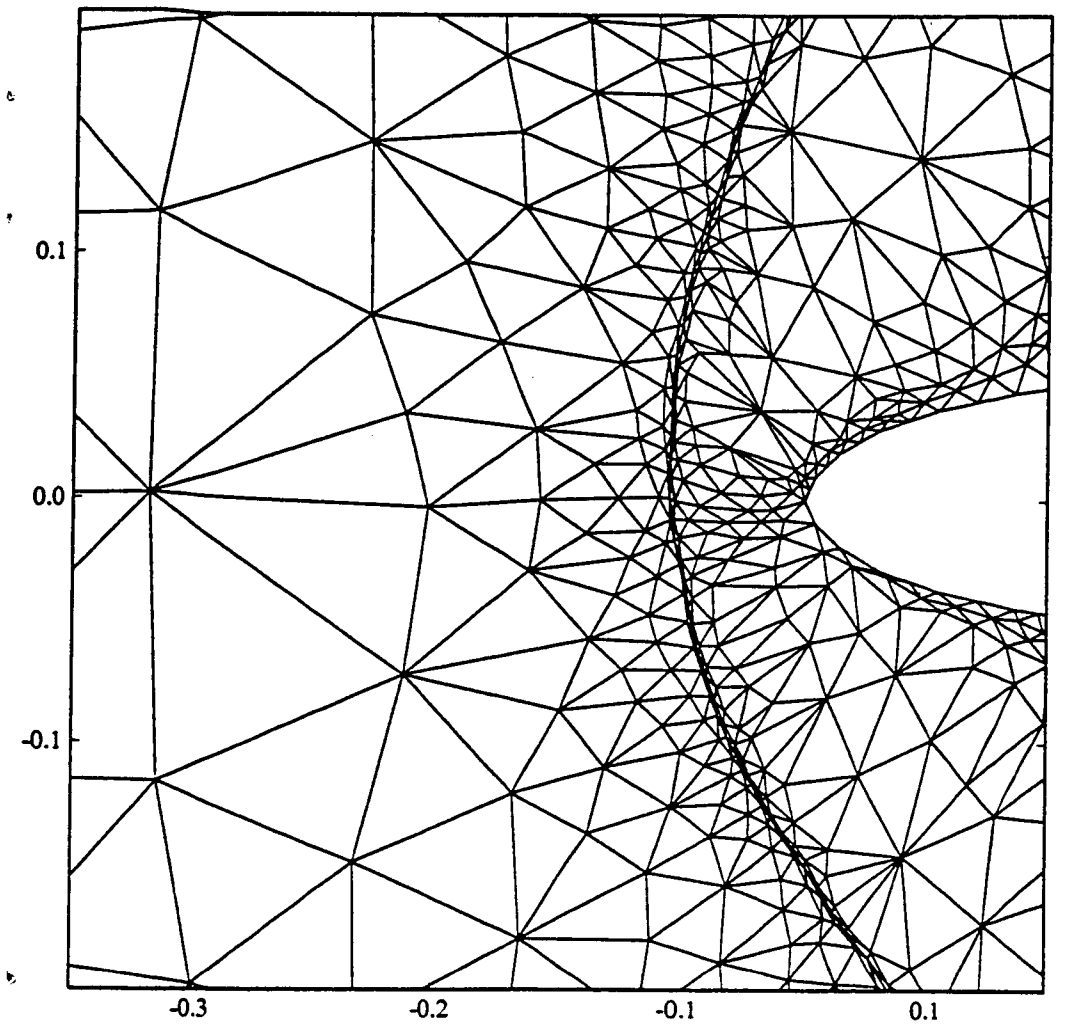

Figure 30 :
Partial view
of Fig. 28

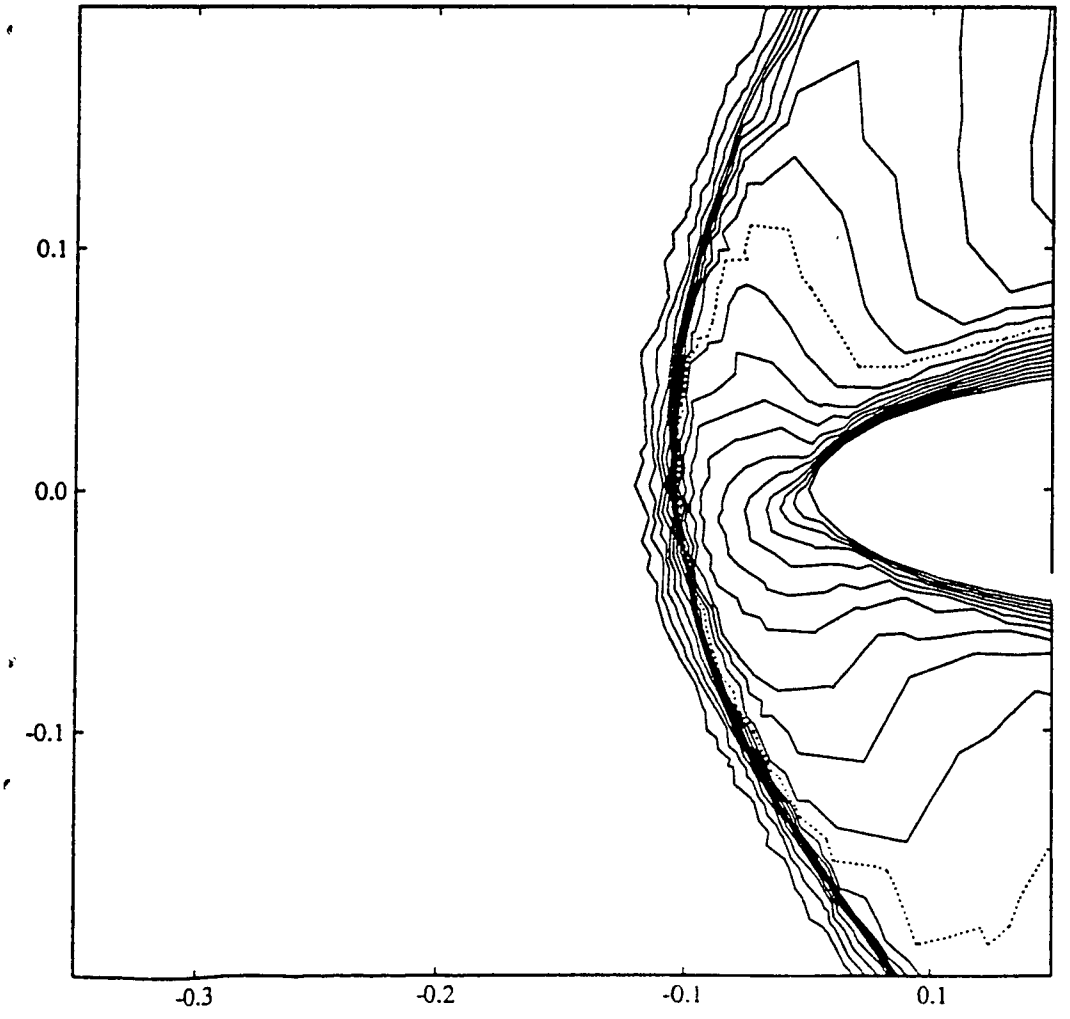

Figure 31 :
Partial view
of Fig. 29